



# A decade long high-resolution wave resource map for Pentland Firth and Orkney Waters - hindcast by two-way coupling of wave-current models

Tian Tan, Vengatesan Venugopal\*

*Institute for Energy Systems, School of Engineering, The University of Edinburgh, The King's Buildings, Colin Maclaurin Road, Edinburgh EH9 3DW, UK*

## ARTICLE INFO

### Keywords:

Wave power resource  
Wave height  
Numerical modelling  
Wave-current interaction  
TOMAWAC  
TELEMAC

## ABSTRACT

Wave energy is a promising renewable resource globally, with the UK leading efforts in regions like Pentland Firth and Orkney Waters. These areas, known for their strong tidal currents and energetic waves, require accurate wave energy resource assessments. This study developed numerical models, including a wave-only and a coupled wave-current model, to simulate combined wave-current conditions over a decade (2014–2023), evaluating the influence of tidal currents. The models assessed interannual, seasonal, and monthly wave resource variations and the impacts of wave-current interactions.

First, a North Atlantic-scale wave-only model was constructed with TOMAWAC spectra wave model to simulate wave conditions without tidal influences and generate wave boundary conditions. Then, a regional wave-current model was developed by coupling TOMAWAC and TELEMAC. This coupled model used the wave boundary conditions from the large-scale North Atlantic model to obtain wave parameters including tidal effects. The North Atlantic wave model was validated against 10 years of continuous wave buoy data across four sites, while the regional wave-current model was verified with 135 days of Acoustic Wave and Current Profiler (AWAC) and Acoustic Doppler Current Profiler (ADCP) deployments, ensuring model reliability.

The results reveal significant spatial and temporal variations in wave energy resources, with pronounced tidal effects. Based on 10 years of data, including tidal currents in the model, substantially decreases mean wave height and mean wave power in the northern and southern regions of the Orkney Islands and Stroma Island in the Pentland Firth. Near Stroma Island, wave height reductions can reach up to 0.5 m (a 25 % reduction compared to the wave-only scenario), and wave power decreases by 6 kW/m (over 50 % reduction). Conversely, wave power increases at tidal inlets such as Pentland Firth, Hoy Mouth, and Westray Firth, with a 10-year average increase of up to 7.7 kW/m (22 %) at Westray Firth. Long-term data indicate that wave-current interactions vary significantly by season, month, and year, with notable changes during winter and high-wave periods. Extreme wave conditions are also amplified by tidal currents, particularly at the tidal inlets within the regional model. The findings could benefit not just the wave energy industry, but also other fields concerned with wave-current dynamics.

## 1. Introduction

The waters around the Pentland Firth and Orkney Water, located to the north of mainland Scotland, are globally recognized as a prime location for wave energy development. The west coast of the Orkney Islands faces the North Atlantic Ocean and experiences predominantly south-westerly winds that travel from eastern Canada or southern Greenland, resulting in significant and consistent swell waves (Vögler and Venugopal, 2013). Also, storms developed over the US East Coast and South Atlantic regions will transform into swell waves when they

arrive at the UK Coastlines. Due to the geographical advantages, the annual mean wave power on the west of the Orkney Islands can be maintained at approximately 31 kW/m (Neill et al., 2017). Leveraging the abundant wave power resources, the European Marine Energy Centre (EMEC) has established two wave energy test sites in this region ([Scale test sites: EMEC: European Marine Energy Centre n.d.](#), [Grid-connected wave test site : EMEC: European Marine Energy Centre n.d.](#)). The test sites offer facilities for wave energy converter developers to deploy their devices and assess their power production capabilities and monitor device survivability for various wave conditions. Some of the

\* Corresponding author.

E-mail addresses: [tian.tan@ed.ac.uk](mailto:tian.tan@ed.ac.uk) (T. Tan), [V. Venugopal](mailto:V.Venugopal@ed.ac.uk).

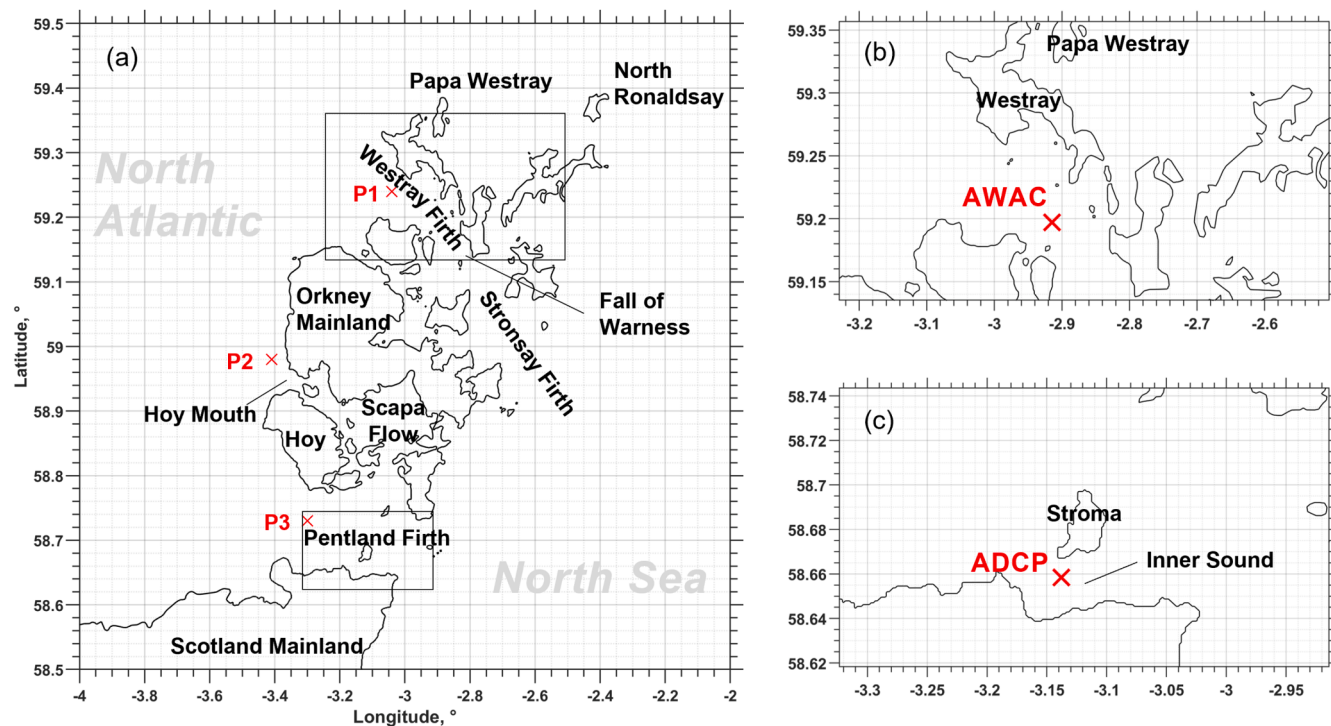


**Fig. 1.** Coastalines or shorelines of the Pentland Firth and Orkney Waters. (a) Overview of the entire PFOW region. (b) Location of the AWAC deployment in Westray Firth, (c) Location of the ADCP deployment in Pentland Firth.

recent activities have been undertaken by the leading wave energy developers around the world, such as LAMINARIA ([Laminaria: EMEC: European Marine Energy Centre n.d.](#)), AWS ([AWS Ocean Energy: EMEC: European Marine Energy Centre n.d.](#)), MOcean ([Mocean Energy: EMEC: European Marine Energy Centre n.d.](#)), and CorPower ([CorPower Ocean: EMEC: European Marine Energy Centre n.d.](#)). Therefore, an accurate wave resources assessment in this region would be very meaningful in the development of the wave energy industry.

In addition to its rich wave resources, the Orkney and Pentland region is also known for having some of the fastest tidal currents in the world. As shown in Fig. 1(a), with over 70 islands, the geographic features of the Orkney create favourable conditions for rapid tidal flows, with currents often exceeding 2.5 m/s ([Neill et al., 2017](#)). Specifically for the Pentland Firth, which serves as a natural channel connecting the North Atlantic and the North Sea, tidal speeds can surpass 5 m/s ([Saruwatari et al., 2013](#)). Consequently, Orkney is a region where strong waves and tidal currents coexist, leading to inevitable wave-current interactions (WCI), which theoretically can significantly impact wave parameters through both wave kinematics and dynamics ([Wolf and Prandle, 1999](#)). Kinematically, tidal currents affect wave dispersion (Doppler shifts) and change wavelength or frequency in downstream/upstream flows. Dynamically, WCI influences wave energy and action conservation, explaining variations in wave height or average levels. A well-known example of WCI affecting wave parameters is along the southeastern coast of South Africa, where the Agulhas Current creates dangerous rogue waves that pose serious threats to vessels ([The Treacherous and Productive Seas of Southern Africa 2017](#)). Similarly, in the Albufeira lagoon, Portugal, the currents can increase the wave height at the mouth of the tidal inlet up to 20 % ([Dodet et al., 2013](#)). For the Orkney and Pentland region in the UK, the wave parameters (including heights, periods, and directions) are found to be strongly modulated by tidal currents ([Venugopal and Vögler, 2020; Venugopal et al., 2018](#)). In some areas, wave heights may increase by 150–200 %, and wave power can rise by over 100 kW during certain tidal phases ([Saruwatari et al., 2013](#)). Despite the growing evidence and theoretical understanding of WCI, there remains a widespread lack of consideration

for tidal effects in wave energy assessments, including the Orkney waters.

Before delving into studies on WCI, it is essential to understand the general methods used to assess wave resources. Over recent decades, several estimation methods have been proposed, but the most popular and accurate approach remains numerical simulation using spectral wave models, such as WAM ([Group, 1988](#)), WAVEWATCH III ([Tolman, n.d.](#)), SWAN ([Booij et al., 2015](#)), and MIKE21-SM ([DHI 2024](#)). For applications specifically focused on Scotland or the waters around the Orkney Islands, [Bertotti and Cavalieri \(2012\)](#) developed a WAM wave model with a resolution of 1/50° (approximately 2 km), which highlighted the importance of using a two-dimensional input wave spectrum at the model grid boundaries. Similarly, [Gleizon and Woolf \(2013\)](#), as well as [Gleizon and Murray \(2014\)](#), constructed wave models with SWAN, applying the two-dimensional wave spectrum from the large-scale WaveWatch III model as boundary conditions. They demonstrated that swell could propagate over long distances, affecting wave energy levels in the central area of the model. [Neill et al. \(2015\)](#) developed a regional-scale SWAN wave model for the Orkney waters, with a two-dimensional wave boundary derived from a coarser North Atlantic SWAN model. This study highlighted interannual and seasonal variability in wave resources over a ten-year period (2003–2012). [Venugopal and Nemalidinne, \(2015\)](#) and [Venugopal et al. \(2017\)](#) utilized the MIKE21 suite to create a North Atlantic scale model with finer subgrids for Scottish and Orkney waters. They achieved a high Pearson's correlation coefficient (over 0.94) for significant wave heights at five validation points across one year. Additionally, [Lavadas et al. \(2017\)](#) applied the SWAN model to generate an 11-year (2004–2014) wave dataset, refining previous wave charts and resource estimates.

While wave modelling is well-researched, studies considering the tidal effects are relatively limited. [Saruwatari et al. \(2013\)](#) used tidal data obtained from the MOHID Water Modelling System as input for the SWAN model to study the impact of tidal currents around Orkney Waters. Their results showed significant differences in wave parameters with and without tidal forcing; however, the coarse mesh resolution and short simulation period limited its application for practical energy

assessments. In the Adriatic Sea, Italy, a two-way coupled ROMS and SWAN model was developed, revealing that neglecting the tidal currents could lead to wave power estimation errors of up to 30 % (Benetazzo et al., 2013; Barbariol et al., 2013). Similarly, Venugopal et al. (Venugopal and Nemalidinne, 2015; Venugopal and Nemalidinne, 2014) developed a two-way coupled wave-current model using the commercial MIKE 21 and MIKE 3 for the Orkney region, incorporating wave boundary conditions from a North Atlantic wave model (Venugopal and Vögler, 2020; Venugopal et al., 2018), which demonstrated clear wave modulation due to tidal effects. Hopkins et al. (2016) developed a coupled SWAN-Delft3D model for the southern shore of Martha's Vineyard, US, and found that tidal currents modulated wave direction by  $\pm 35^\circ$ , primarily due to tidal refraction rather than water level changes. Guillou (2017) used TELEMAC 2D results in the SWAN model (in one-way coupled model) and observed that significant wave height at the northern entrance of Fromveur Strait in France varied by up to 30 % with tidal effects, with wave power increasing by >100 %.

Despite these advancements, gaps persist. Most wave models undergo extensive calibration, often exceeding a month or even a year at multiple locations. In contrast, wave-current coupled models rarely receive such thorough validation, often limited to brief weekly calibrations. Furthermore, wave-current coupled models are typically applied over short timeframes, lacking long-term statistics to reveal monthly or seasonal tidal effects. This limitation is likely due to the significant computational resources required for such models. One unique example of long-term tidal influence simulation is Webb et al. (2020), who conducted a 21-year WAVEWATCH III simulation for Japan, incorporating tidal currents from JCOPE2. While their research provided valuable insights into long-term wave-current interactions, it lacked wave calibration under tidal effects, affecting the reliability of the results. Additionally, their simulation required 35 days of supercomputer time, making replication in other regions challenging.

The present study addresses these gaps by developing a two-way coupled wave-current model, validated with field measurements spanning several months across different locations. The model generates a comprehensive 10-year (2014–2023) dataset of wave parameters including tidal effect, providing a long-term insight into the tidal current effects on wave resources. By applying open-source software with efficient computational requirements, this approach ensures replicability in other places. Specifically, the feasibility of this research relies on using the TOMAWAC wave model and the TELEMAC tidal flow model within the open-source Telemac system. TOMAWAC (TOMAWAC - Wave propagation in coastal areas n.d.) is a reliable third-generation spectral wave model, capable of handling wave simulations for oceans, inland seas, and coastal areas. While less popular compared to the previously mentioned wave models, partly due to its command-line interface and its common use as a submodule of the TELEMAC flow model rather than a standalone solution, TOMAWAC has actually demonstrated strong predictive accuracy. For instance, in the Iroise Sea, France, it outperformed SWAN in estimating wave power due to its direct calculation of total energy flux, avoiding the approximations inherent in SWAN's default methods that can underestimate wave power by up to 15 % (Guillou, 2015). Regarding the TELEMAC flow model, it has been widely applied in the Orkney Waters and is proven to be able to accurately simulate the tidal flows in this region (Abdul Rahman and Venugopal, 2015; Perez Ortiz, 2013). The coupling between TOMAWAC and TELEMAC requires minimal parameter adjustments, shares the same mesh and boundary conditions, and enables efficient simulations; however, this is the first research that used the TOMAWAC-TELEMAC system in two-way coupled mode and applied it to the Orkney Islands and Pentland Firth waters.

In this study, the coupled model was validated over a cumulative 135 days across two geographically distinct sites in the Orkney Waters, showcasing its generalization capabilities. A subsequent 10-year simulation using both wave-only and wave-current coupled models was conducted to account for tidal influences and assess long-term impacts

on wave parameters. The results include a high-resolution wave resource map that examines interannual, inter-seasonal, inter-monthly, and extreme wave conditions, offering comprehensive insights into tidal effects. In the following sections, this paper outlines the theoretical foundations of the numerical models and provides evidence of their effectiveness. Subsequently, it presents a detailed 10-year wave map, emphasizing the spatial and temporal impacts of tidal currents on wave parameters.

## 2. Methodology

This section provides the theoretical framework underlying the TOMAWAC and TELEMAC models based on their technical manuals. The fundamental mechanisms governing wave-current coupling between these models are described, detailing into how they simulate combined wave and tidal flow dynamics effectively.

### 2.1. TOMAWAC wave model

TOMAWAC simulates wave propagation by solving the time-dependent wave action balance equation in the Cartesian coordinate system ( $x, y$ ) (Awk, 2019),

$$\frac{\partial N}{\partial t} + \frac{\partial(\dot{x}N)}{\partial x} + \frac{\partial(\dot{y}N)}{\partial y} + \frac{\partial(k_x N)}{\partial k_x} + \frac{\partial(k_y N)}{\partial k_y} = Q(k_x, k_y, x, y, t) \quad (1)$$

where the  $(k_x, k_y)$  in the balance equation represent the wave number  $k$  vector along the  $x$  and  $y$  directions;  $N$  is the directional spectrum of wave action density and is usually used to describe the waves in unsteady or inhomogeneous medium. The definition equation of  $N$  is

$$N(\sigma, \theta) = \frac{F(\sigma, \theta)}{\sigma} \quad (2)$$

in which  $F$  is the directional spectrum of the variance density;  $\sigma$  and  $\theta$  represents relative or intrinsic angular frequency and the wave propagation directions in radians, respectively.  $F$  is furtherly defined by  $F(\sigma, \theta) = E(\sigma, \theta)/\rho g$ , with  $E$  is the directional spectrum,  $\rho$  is the water density, and  $g$  is the gravity acceleration.

Eq. (1) demonstrates that the wave action is preserved to within the source and sink terms  $Q$ , which in this study is described by

$$Q = Q_{in} + Q_{ds} + Q_{nl} + Q_{bf} + Q_{br} + Q_{ds,cur} \quad (3)$$

where  $Q_{in}$  is wind input for wave generation,  $Q_{ds}$  is white capping induced interactions,  $Q_{nl}$  is non-linear quadruplet interactions,  $Q_{bf}$  is bottom friction induced energy dissipation,  $Q_{br}$  is bathymetric breaking induced energy dissipation,  $Q_{ds,cur}$  represent the wave blocking effects when waves meet strong adverse current, which in this study is only enabled when coupling with the TELEMAC tidal flow model.

Specifically, the way to simulate this enhanced breaking dissipation by strong current relies on the Westhuyzen method (van der Westhuyzen, 2012)

$$Q_{ds,cur} = -C_{ds,cur} \max \left[ \frac{C_\sigma}{\sigma}, 0 \right] \left( \frac{B(k)}{B_r} \right)^{p_0/2} F(f, \theta) \quad (4)$$

in which the spectral saturation level  $B(k)$  as a ratio of the threshold level  $B_r$  determines the dissipation level and can be enhanced by the factor  $C_\sigma/\sigma$ . When  $B(k) > B_r$  wave breaks and the function to determine the exponent of  $p_0$  can be found in (Awk, 2019; van der Westhuyzen et al., 2007); while when  $B(k) < B_r$  there is no breaking by having  $p_0 = 0$ . In this study, the most critical parameter for determining enhanced breaking is  $C_{ds,cur}$  after a detailed sensitivity analysis. Notably, this value is far larger than the default value of 0.65, which would result in overestimated wave heights. A similar finding of using a value of 5 was reported in (Dodet et al., 2013). The remaining model setup parameters

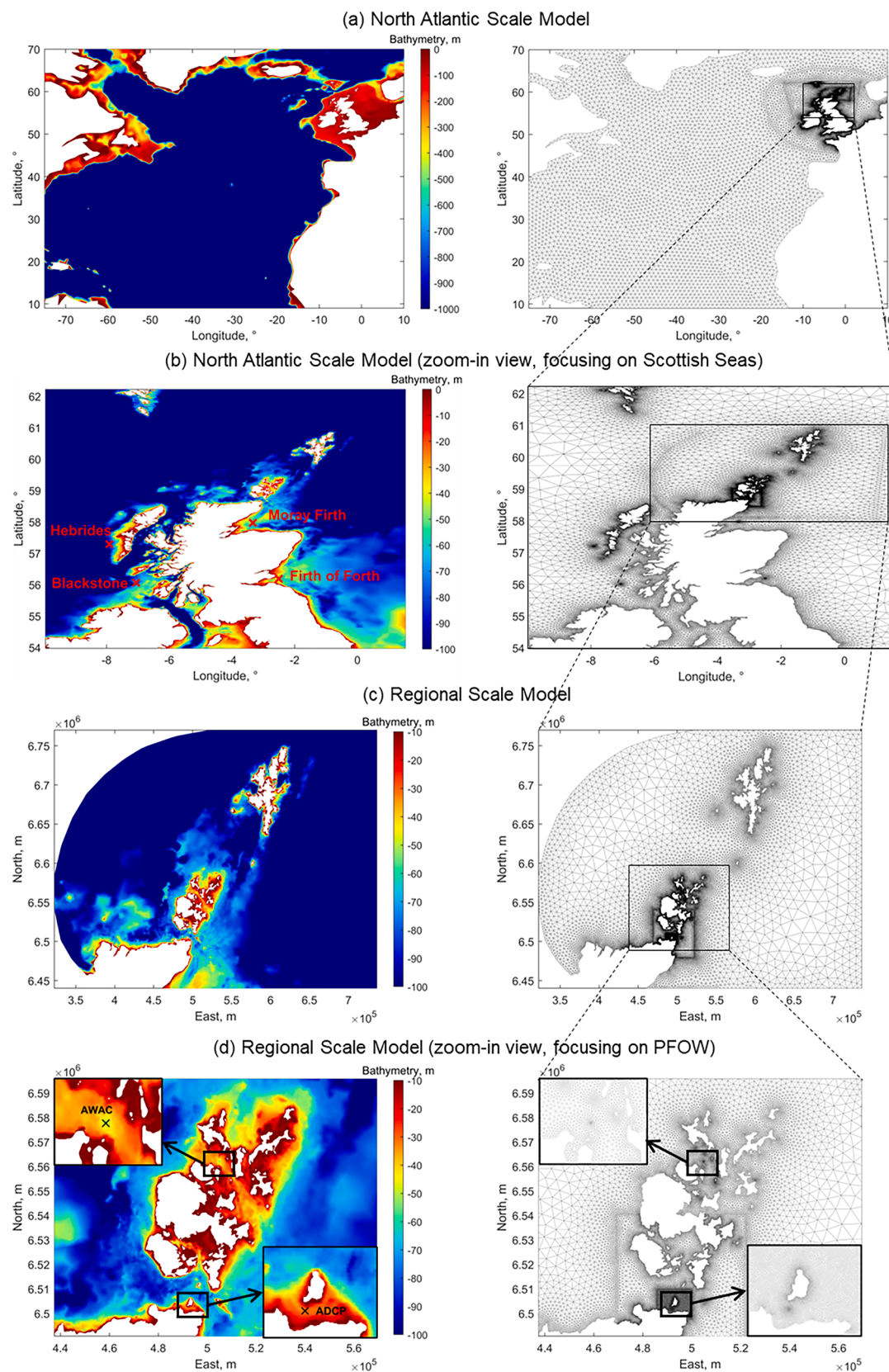


**Fig. 2.** Bathymetry and mesh of the North Atlantic scale and regional scale model. (a) and (b) are presented in the latitude/longitude system. (c) and (d) are presented in the UTM coordinate system.

are presented in Section 3.1.1.

The wave parameters, such as the significant wave heights ( $H_{m0}$ ), zero-crossing wave periods ( $T_z$ ), and the peak wave periods ( $T_p$ ) are directly output from the model, which are derived through the spectra moment methods. The details may be found in the TOMAWAC manual (Awk, 2019). It is worth highlighting the unit wave power rate or the wave energy flux ( $P$ ), which is also a direct output of the model, is computed from the total energy transport (Guillou, 2015)

$$P = \rho g \int_0^{2\pi} \int_0^{\infty} C_g F d\sigma d\theta \quad (5)$$

where  $C_g$  is the relative or intrinsic wave group velocity. Notably, though the numerical resolution of equations used the relative or intrinsic frequency (i.e., the frequency being observed in a coordinate system moving at the velocity of current, for which linear wave theory applies), the final output of the model is transferred to the absolute frequency (i.e., the frequency observed from a fixed coordinate system) and can be directly used in the real world.

## 2.2. TELEMAC flow model

TELEMAC 2D and 3D are all designed for the simulation of the flow velocity field. This study utilized the TELEMAC 3D module with two layers only (i.e., only bottom and surface layers), with no intermediate layers, with the aim of accelerating the simulations for longer-term purposes.

The TELEMAC 3D solves the 3D Navier-Stokes equations with a free surface, which is expressed by (Awk, 2019),

$$\frac{\partial u}{\partial x} + \frac{\partial v}{\partial y} + \frac{\partial w}{\partial z} = 0 \quad (6)$$

$$\frac{\partial u}{\partial t} + u \frac{\partial u}{\partial x} + v \frac{\partial u}{\partial y} + w \frac{\partial u}{\partial z} = -g \frac{\partial u}{\partial x} + v \Delta(u) + F_x \quad (7)$$

$$\frac{\partial v}{\partial t} + u \frac{\partial v}{\partial x} + v \frac{\partial v}{\partial y} + w \frac{\partial v}{\partial z} = -g \frac{\partial v}{\partial y} + v \Delta(v) + F_y \quad (8)$$

$$p = p_{atm} + \rho_0 g(z_s - z) + \rho_0 g \int_z^{z_s} \frac{\Delta \rho}{\rho_0} dz' \quad (9)$$

in which,  $u$ ,  $v$ , and  $w$  are the three-dimensional components of velocity;  $x$ ,  $y$  and  $z$  are the 3D coordinates,  $g$  is the acceleration due to gravity,  $\nu$  is the kinematic viscosity,  $F_x$  and  $F_y$  are the source terms,  $p$  and  $p_{atm}$  are the total pressure and atmospheric pressure respectively,  $z_s$  is the free surface elevation,  $\rho_0$  and  $\Delta \rho$  are the reference density and the variation of density around it, respectively.

During the wave-current coupling, the updated values of the wave driving forces  $F_x$  and  $F_y$  are passed from TOMAWAC to the TELEMAC, while the current velocity and water depth are transferred from TELEMAC to TOMAWAC. Further details of the numerical model may be found in (Awk, 2019). Some of the calibration parameters associated with the TELEMAC model has been found through an iteration process; however, a few parameters are left out at their default values. Further details are given in Section 3.2.1 below.

## 3. Numerical modelling

Two numerical models are established in this study: (1) a North Atlantic wave-only model using TOMAWAC, developed to simulate wave conditions without tidal effects and to provide high-resolution boundary conditions for the subsequent regional model; and (2) a regional wave-current coupled model by TOMAWAC and TELMEAC, designed to simulate combined wave-current interactions. This section

presents the setup, calibration, and validation results for both models.

Before detailing these aspects, it is important to justify the rationale for developing a bespoke North Atlantic wave model instead of directly using ECMWF ERA5 wave data (Copernicus Climate Change Service (C3S) 2017), which already includes wave heights and spectral information. Although ERA5 data are convenient, their coarse spatial resolution (over 0.5°) provides limited boundary coverage and directional resolution details in particular if the model domain is smaller than the area of grid points covered by ERA5 data. In addition, ERA5 data becomes less suitable for accurately capturing wave dynamics at specific locations of interest, when the point of interest is not exactly lying at the ERA5 grid points. Another key observation was that ERA5 data fails to compare well with measurements at locations close to shallow waters of complex profiles such as the regions considered in this study.

### 3.1. North Atlantic scale wave model

#### 3.1.1. Mesh and set-up

As the North Atlantic wave model spans more than ten UTM zones and is unsuitable to be simulated under the Cartesian coordinates, the simulation therefore operates in a spherical spatial coordinate system (i.e., by latitude and longitude). The simulation domain spans from 10°E to 75°W in longitude and from 9°N to 70°N in latitude, covering the North Atlantic and the British Isles, as shown in Fig. 2(a). To conserve computational resources, the model employs a lower resolution in the North Atlantic, with a maximum grid size of 1° (approximately 100 km). As the model approaches the Irish and British Isles, the mesh becomes finer, with a transitional region at a maximum mesh length of 0.5° (around 50 km), further refining to within 0.02° (around 2 km) near coastlines. For model validation sites, which are presented in Fig. 2(b), grid spacing is controlled to within 50 m.

The higher-resolution regional model, used for subsequent wave-current coupling simulation, is fully nested within the North Atlantic model as a sub-grid, as illustrated in Fig. 2(c). It covers the entire Orkney and Shetland region, while the grid resolution in the Orkney waters is finer. For the Westray Firth in Fig. 2(d), coastline resolution is within 300 m, and the smallest mesh size is at the AWAC location, within 50 m. For the Pentland Firth, a nested sub-grid is included around the Stroma Island in order to accurately capture the high-speed tidal currents. The largest mesh size of this region is 200 m, with the finest grid being 30 m at the ADCP site deployed in the inner sound.

The wind data that is used to drive the wave model is obtained from the ECMWF ERA5 reanalysis dataset (Copernicus Climate Change Service (C3S) 2017), with the temporal and spatial resolution of 1 hour and 0.25° × 0.25°, respectively. To simulate wind wave growth, this study employs the Yan's formulation (corresponding to WIND GENERATION = 3 in the TOMAWAC steering file) (Awk, 2019; Yan, 1987), with default coefficient values as proposed by van der Westhuyzen (van der Westhuyzen et al., 2007). In the numerical simulation, each node calculates waves from 36 directions (at 10° intervals), with each direction containing 36 frequency components. The minimum wave frequency is 0.04 Hz, with an increment ratio of 1.08, covering a frequency range of 0.04 - 0.6 Hz (i.e., period range: 25 - 1.67 s). The timestep is set to 600 s.

Outputs from the North Atlantic wave model include wave parameters (e.g.,  $H_{m0}$ , mean wave direction,  $T_m$ ,  $T_p$ , and wave power) and two-dimensional directional wave spectra at specified nodes, the latter of which serve as wave boundary conditions for regional model simulation. With these settings, the model was calibrated using data from 2011 and validated using data from 2016 at multiple sites, as documented in (Tan and Venugopal, 2023). The root mean square error (RMSE), scatter index (SI), and Pearson's linear correlation coefficient (R) values all show good agreement with the corresponding measurements. Due to space constraints, the validation plots are not included in that publication; however, the model's effectiveness is further supported by hindcast comparisons as mentioned below.

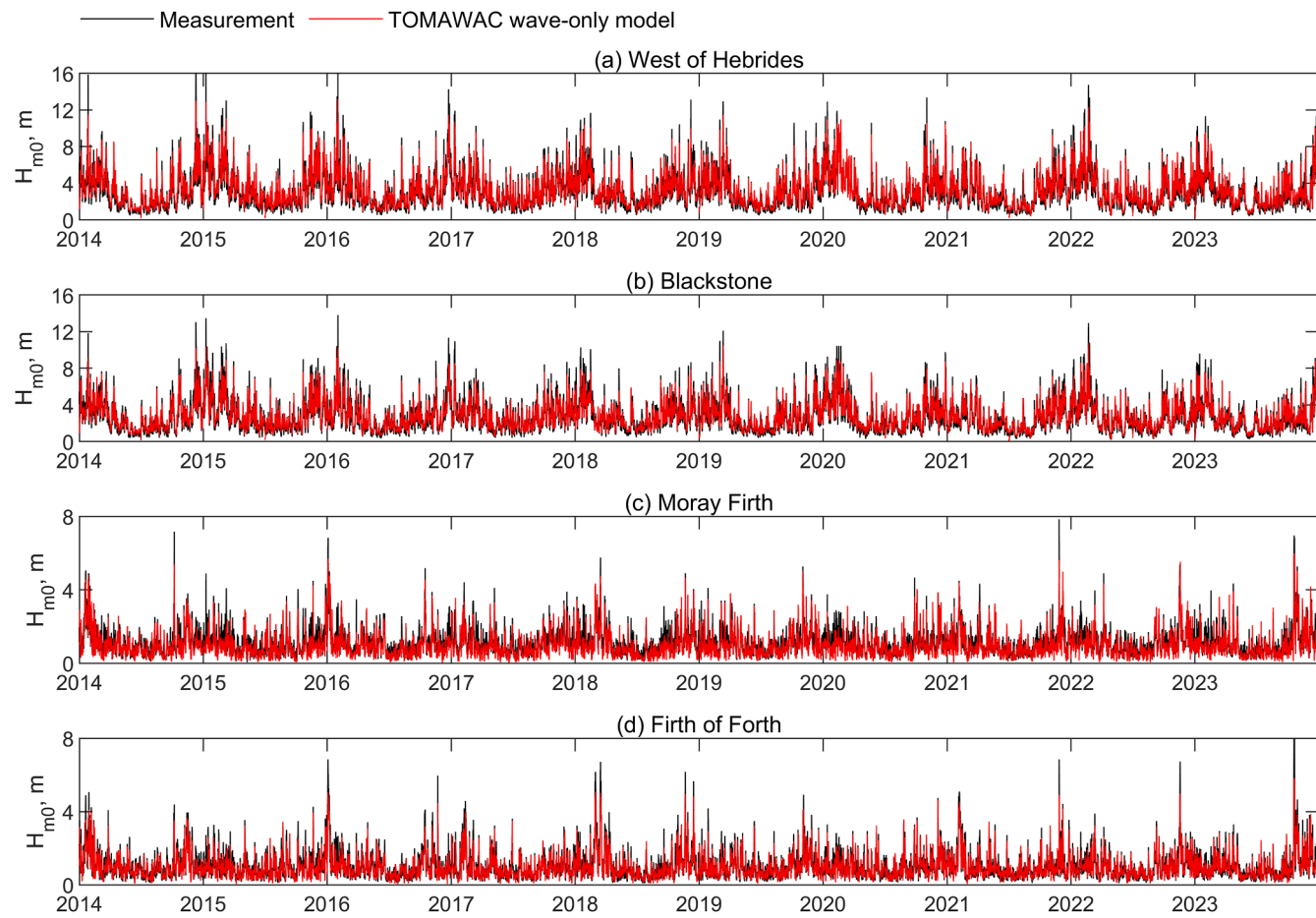


**Fig. 3.** Comparison of significant wave heights  $H_{m0}$  between the North Atlantic scale TOMAWAC wave-only model and wave buoys' measurement, from January 2014 to December 2023.

### 3.1.2. Hindcasting of wave parameters and results verification with buoy data

The effectiveness of the North Atlantic wave model is confirmed by the wave buoys measurements at four sites (see in Fig. 2(b)) around the Scotland, that are the West of Hebrides ( $57^{\circ} 17' 31'' N, 7^{\circ} 54' 50'' W$ ), Blackstone ( $56^{\circ} 3' 43'' N, 7^{\circ} 03' 24'' W$ ), Moray Firth ( $57^{\circ} 57' 59'' N, 3^{\circ} 19' 59'' W$ ), and Firth of Forth ( $56^{\circ} 11' 16'' N, 2^{\circ} 30' 14'' W$ ), provided by the Cefas WaveNet (Cefas - WaveNet interactive map n.d.). These four sites are in the open sea with mitigated tidal current flows, with two sites directly facing the North Atlantic with deep water depth around 100 m, and the others are in the bay region facing the North Sea with relatively shallower water depth around 60 m. The wave buoys' measurements are recorded every 30 min unless the missing data.

Figs. 3–5 present wave parameters hindcast for 10 years (January 2014 to December 2023). The time series of  $H_{m0}$ ,  $T_z$  and  $T_p$  between the North Atlantic TOMAWAC wave model and wave buoy measurements are compared in these plots. Table 1 provides the detailed performance metrics, including Bias, Normalized Bias (i.e., Bias/mean value), RMSE, SI, and the R. It is noted that the R values indicate correlation in trends between the model and measurements, while the Normalized Bias and SI demonstrate the match in absolute values.

The hindcast results of the  $H_{m0}$  and  $T_m$  align very well with the measurements, with the highest R values reaching 0.98 and 0.93, respectively, at the West of Hebrides site. Across all sites, R value exceeds 0.93 for  $H_{m0}$  and 0.83 for  $T_m$ , demonstrating the model's strong accuracy. For  $T_p$ , which is typically harder to match than other wave parameters, the time series closely follow the measurements, accurately capturing annual cycles. At Blackstone and the West of Hebrides, both are deep water sites, the R values for  $T_p$  are at 0.85 and the SI values are

even within 0.15, showcasing the model's ability at deep water sites.

However, at two sites facing the North Sea with shallower waters and weaker winds, particularly the Moray Firth, the model shows comparatively lower performance for  $T_p$ , as suggested by the metrics. This could be attributed to geographic factors that complicate simulation and, more importantly, frequent data gaps in measurements at these locations, making precise matching more challenging. Despite these limitations, the model demonstrates strong performance for  $H_{m0}$  and  $T_m$  at Moray Firth, further supporting its overall effectiveness. Notably, similar challenges in simulating  $T_p$  at Moray Firth have been observed in other models, such as MIKE 21 (Venugopal and Nemalidinne, 2015), where the R value was as low as 0.39 in 2010. In comparison, the performance of the TOMAWAC model in this study is relatively better.

With the model's effectiveness validated over 10 years across various locations, its ability to capture inter-annual variability is well-supported. In addition, since wave power is closely tied to wave heights and periods, the strong match in these parameters confirms the reliability of the hindcast data for wave power estimation.

### 3.2. Regional scale wave-current coupled model

#### 3.2.1. Model set-up

The mesh configuration for the regional model was introduced in Section 3.1. This section focuses on parameter settings for the wave-current coupled model, which integrates the TOMAWAC wave model and the TELEMAC flow model. These two independent models are linked through a series of parameters, enabling data exchange at each coupling step.

The wave model parameters are generally consistent with those used

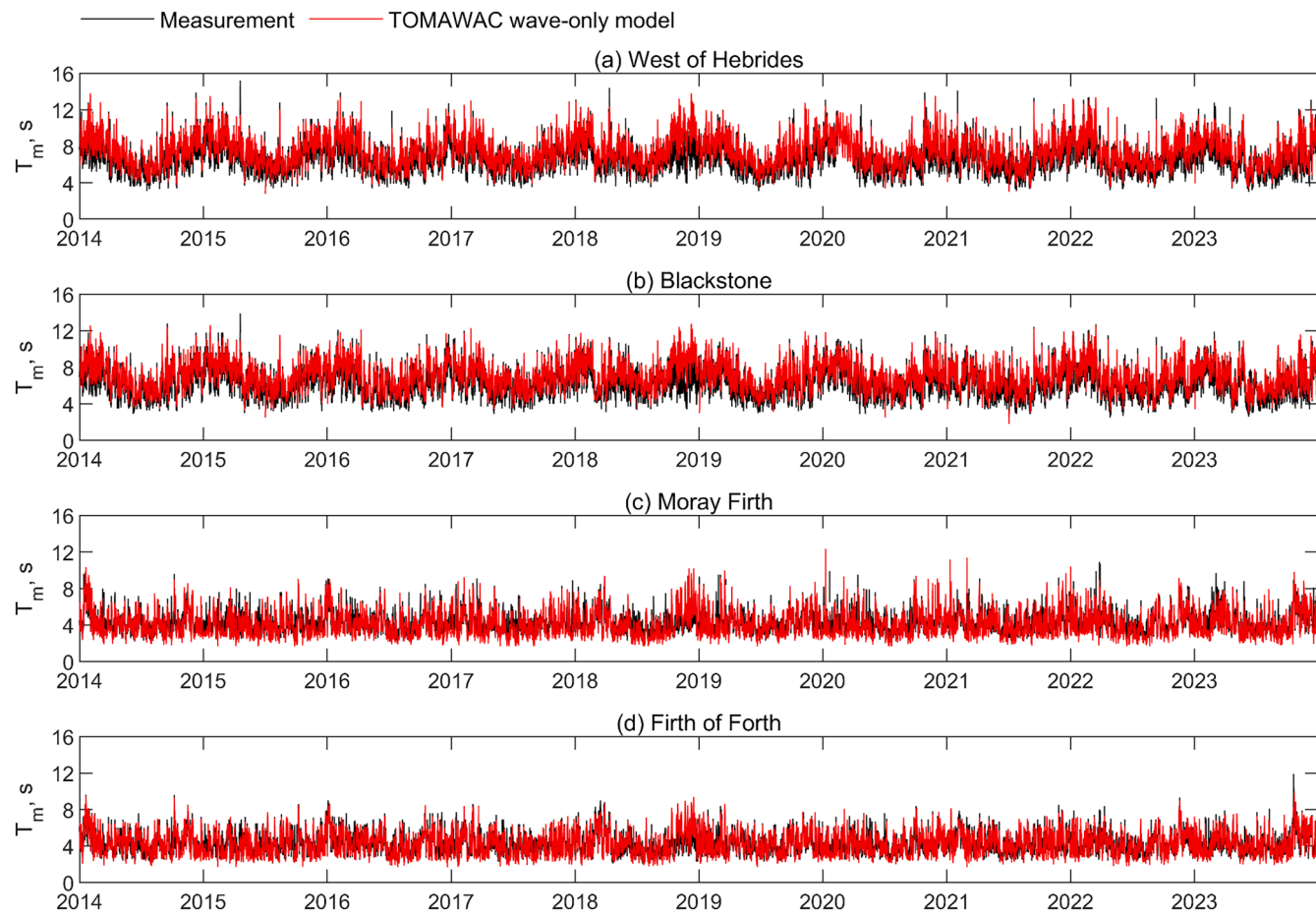


**Fig. 4.** Comparison of mean wave periods  $T_m$  between the North Atlantic scale TOMAWAC wave-only model and wave buoys' measurement, from January 2014 to December 2023.

in the North Atlantic model, with wind data sourced from ECMWF ERA5. To ensure stability in the wave-current coupling and prevent simulation errors, the timestep for the wave model is reduced to 300 s.

For the TELEMAC flow model, the global TPXO9 version 4 tidal harmonics database (Egbert and Erofeeva, 2002) provides prescribed boundary conditions for tidal evolution. This includes the tidal elevation amplitude and phase file (*h\_tpox9.v4a*) and the tidal current velocity components file (*u\_tpox.v4a*). The TPXO9 global tidal model includes 15 tidal constituents for sea surface elevation and transport. These consist of eight primaries (M2, S2, N2, K2, K1, O1, P1, Q1), two long-period (Mf, Mm), and three non-linear (M4, MS4, MN4) tidal constituents. The bottom friction is modelled using the Chezy method with a constant value of 66 across the computational domain. The mixing vertical length model is chosen for turbulence. The tidal flats (areas that become intermittently dry and wet) are included from the active computations. Wind forcing is not considered in the flow model, as the only external momentum input comes from the wave-induced forces. The Coriolis effect is also neglected due to the limited spatial extent of the regional model. The flow model operates with a simulation timestep of 5 s, while the wave-current coupling is performed every 300 s.

### 3.2.2. Model validation

The tidal currents and waves simulation results from the coupled wave-current model were calibrated and validated using field measurements collected in typically wave-current environments: (1) Acoustic Wave and Current Profiler (AWAC) deployed at the Westray Firth, and (2) Acoustic Doppler Current profiler (ADCP) deployed at the Inner Sound in Pentland Firth, as shown in Fig. 2 (d). The AWAC data were collected over 77 days, from 19 July to 4 October 2016, with

measurements provided at 30-min intervals. The ADCP data spanned 58 days, from 15 October to 12 December 2017, with a sampling frequency of 2 Hz. For comparison with the model, the ADCP data were averaged to match the model's 10-minute timestep. The numerical model results are presented as time series in Figs. 6 and 7 for Westray Firth and Pentland Firth, respectively, with a summary of the model's performance metrics provided in Table 2.

**3.2.2.1. Tidal parameters.** The depth-averaged tidal current velocities produced by the numerical model were validated against field measurements at 0.4 times the total depth from the seabed. This depth is considered a reliable approximation for the averaged velocity in TELEMAC, assuming a vertical tidal profile that follows the 1/7 power law (Lewis et al., 2017). With this assumption, the model demonstrated an excellent match with the depth-averaged tidal flow speeds at Westray Firth and Pentland Firth, achieving R values of 0.94 and 0.93, respectively. Notably, the maximum tidal speeds observed during the validation period exceeded 2.5 m/s at Westray Firth and reached up to 5 m/s at Pentland Firth, further confirming the energetic tidal flows in these regions.

To provide a broader understanding of the tidal current conditions in Pentland Firth and Orkney Waters, a map showing the annual maximum depth-averaged tidal speeds for the year 2017 was generated and is presented in Fig. 8. The fastest tidal currents are concentrated in the Pentland Firth, particularly in the northern and southern regions around Stroma Island, where speeds exceed 5 m/s across a wide area. Other areas with significant tidal currents include Westray Firth, Stronsay Firth, and the northern edges of the Orkney Islands (around Papa Westray and North Ronaldsay), where speeds surpass 3 m/s.

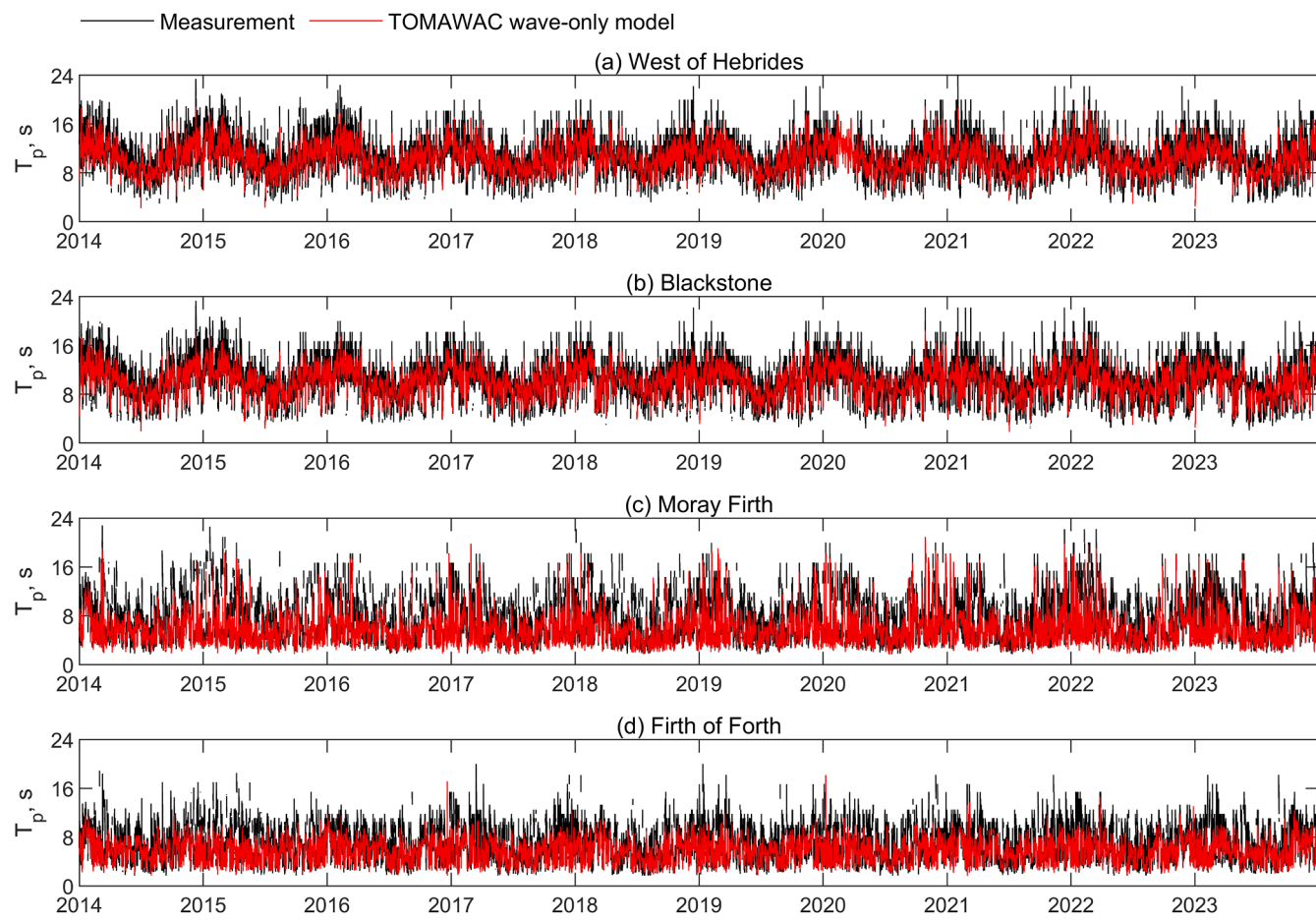


**Fig. 5.** Comparison of peak wave periods  $T_p$  between the North Atlantic scale TOMAWAC wave-only model and wave buoys' measurement, from January 2014 to December 2023.

**Table 1**

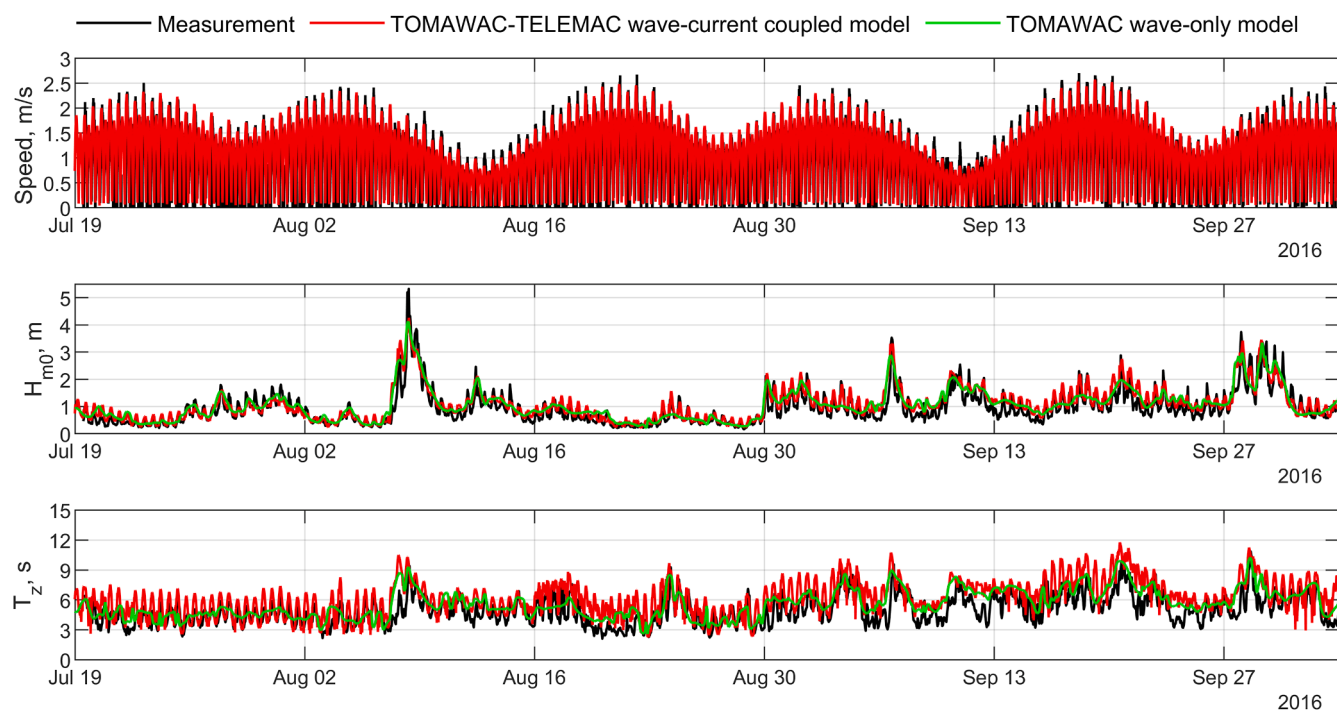
Metrics of the North Atlantic scale TOMAWAC wave-only model, from January 2014 to December 2023.

Location	Parameter	Mean model (real value)	Bias	Normalized Bias	RMSE	SI	R
West of Hebrides	$H_{m0}$ , m	3.03 (3.23)	-0.20	-0.06	0.44	0.14	0.98
	$T_m$ , s	6.79 (7.43)	-0.65	-0.09	0.90	0.12	0.93
	$T_p$ , s	10.97 (10.58)	0.38	0.04	1.42	0.13	0.85
Blackstone	$H_{m0}$ , m	2.66 (2.74)	-0.08	-0.03	0.41	0.15	0.97
	$T_m$ , s	6.43 (7.02)	-0.60	-0.08	0.89	0.13	0.91
	$T_p$ , s	10.62 (10.31)	0.31	0.03	1.51	0.15	0.85
Moray Firth	$H_{m0}$ , m	1.07 (0.98)	0.09	0.10	0.27	0.27	0.93
	$T_m$ , s	4.16 (4.10)	0.07	0.02	0.75	0.18	0.83
	$T_p$ , s	7.12 (5.80)	1.32	0.23	3.11	0.54	0.57
Forth of Firth	$H_{m0}$ , m	1.00 (0.99)	0.02	0.02	0.20	0.20	0.96
	$T_m$ , s	4.20 (4.28)	-0.07	-0.02	0.64	0.15	0.87
	$T_p$ , s	6.74 (5.90)	0.84	0.14	2.08	0.35	0.64

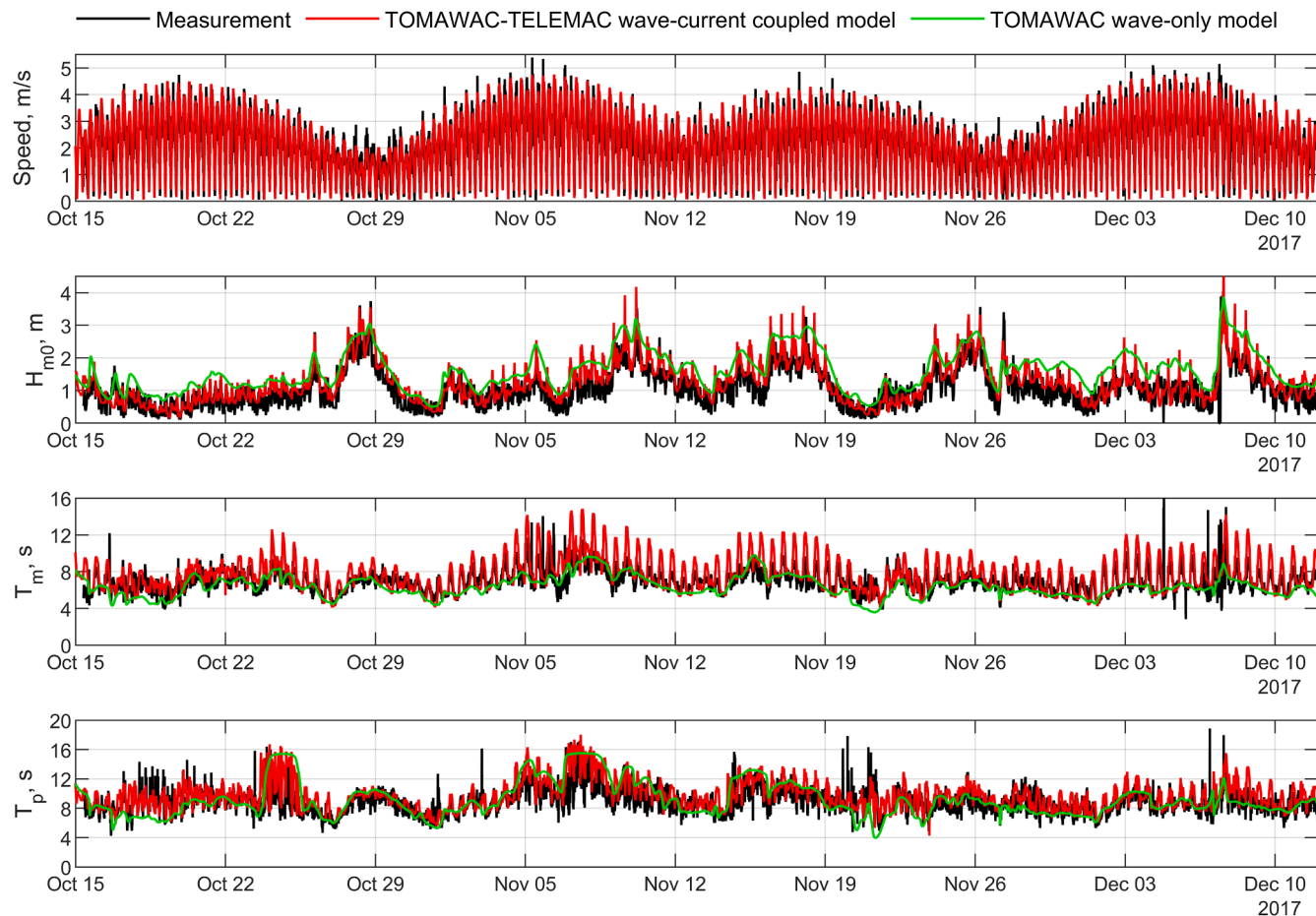
Additionally, Fig. 8 includes maps of tidal conditions during two phases of a Spring Tide on November 6, 2017 - Flood flow (08:20); showing currents flowing from the North Atlantic into the Pentland Firth, and Ebb flow (15:20); showing currents flowing toward the North Atlantic. It is observed that during the ebb phase, the area with tidal speeds exceeding 4 m/s in the Pentland Firth is larger compared to the flood phase, confirming the phenomenon of tidal asymmetry in this region (Neill et al., 2014).

**3.2.2.2. Wave parameters.** With the tidal currents accurately simulated, the wave parameters can now be analysed. Figs. 6 and 7 compare the results of the North Atlantic wave-only model with the wave-current

coupled model and field measurements. The wave-current coupled model (plots with red colour lines) and site measured data (black lines) both exhibit clear periodic fluctuations corresponding to the tidal cycle. In contrast, the wave-only results (light green lines) show a relatively flat curve, ignoring the compelling evidence of tidal modulation effects seen in the measurements. At Westray Firth, the wave-current coupled model closely tracks the measured data, achieving an R value of over 0.92 for  $H_{m0}$ , demonstrating excellent agreement. At the Pentland Firth, the R value for  $H_{m0}$  is slightly lower at 0.85. This is expected, as the Pentland Firth data exhibit high-frequency fluctuations, which may be attributed to several factors: (1) shallower water depth but with much faster tidal currents compared to Westray Firth, leading to increased



**Fig. 6.** Comparison of tidal speed,  $H_{m0}$ , and  $T_z$  between the regional scale TOMAWAC-TELEMAC wave-current coupled model and AWAC measurement recorded at the Westray Firth, from July 19 to October 14, 2016 (77 days).

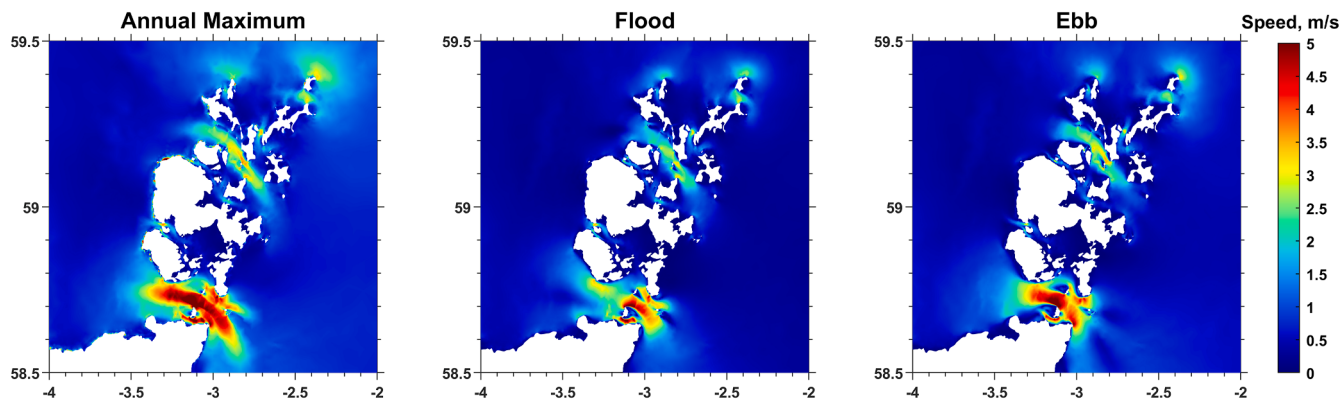


**Fig. 7.** Comparison of tidal speed,  $H_{m0}$ ,  $T_m$ , and  $T_p$  between the regional scale TOMAWAC-TELEMAC wave-current coupled model and ADCP measurement recorded at the Pentland Firth, from October 15 to December 5, 2017 (58 days).

**Table 2**

Metrics of the regional scale TOMAWAC-TELEMAC wave-current coupled model.

Location	Parameter	Mean model (real value)	Bias	Normalized Bias	RMSE	SI	R
Westray Firth	Speed, m/s	1.13 (1.10)	0.03	0.03	0.22	0.25	0.94
	$H_{m0}$ , m	1.09 (0.95)	0.14	0.14	0.30	0.31	0.91
	$T_z$ , s	6.20 (4.95)	1.26	0.25	1.73	0.35	0.72
Pentland Firth	Speed, m/s	2.25 (2.07)	0.17	0.08	0.46	0.22	0.93
	$H_{m0}$ , m	1.24 (1.08)	0.16	0.14	0.37	0.34	0.85
	$T_m$ , s	7.66 (6.94)	0.73	0.10	1.42	0.20	0.76
	$T_p$ , s	9.67 (8.90)	0.78	0.09	1.76	0.20	0.63

**Fig. 8.** Tidal speed atlas of Pentland Firth and Orkney Waters. Left: annual maximum speed of the year 2017. Middle: speed during the flood phase (November 5, 2017, 20:00:00). Right: speed during the ebb phase (November 5, 2017, 14:30:00).

wave-breaking events, and (2) wave parameters are not directly measured but calculated from surface elevation data using spectral methods (Coles et al., 2018; Tan et al., 2023; Tan and Venugopal, 2024). This process can incorporate turbulence or environmental noise, amplifying fluctuations in the final wave parameters. Despite these challenges, both  $H_{m0}$  and  $T_m$  closely follow the modulations. Even the  $T_p$  shows good alignment with an R value of 0.63 and SI of 0.2.

These results indicate the wave-current coupled model's robustness in simulating wave parameters under the influence of tidal currents, even in complex environments like the Pentland Firth.

#### 4. Further analysis and discussions

In the above sections, the effectiveness of both waves only model and the coupled wave-current model, in predicting wave and current parameters and their combined effect is demonstrated. This section focuses on further analysis of wave parameters under the influence of tidal currents. The analysis focuses on the Orkney regions, P1, P2 and P3 (see Fig. 1), with the map zoomed in to the area between 58.5°N - 59.5°N latitude and 2°W - 4°W longitude. Three locations on the west side of the Orkney Islands and within the Pentland Firth are selected for detailed analysis:

- P1: Located at the tidal inlet of the Westray Firth, where the maximum tidal speed is around 1.5 m/s.
- P2: Positioned 700 m westward of the EMEC Billia Croo wave test site on the west side of the Orkney Mainland, with a maximum tidal speed of around 0.4 m/s.
- P3: Situated at the mouth of the tidal inlet of the Pentland Firth, where the maximum tidal speed is around 2.2 m/s.

##### 4.1. Inter-annual analysis

The inter-annual analysis examines annual mean wave heights and

wave power from 2014 to 2023, offering insights into common characteristics and variability over the 10-year scale. This section first describes the spatial characteristics of wave resource distribution and then compares results between the wave-current coupled model and the wave-only model to assess the impact of tidal currents.

##### 4.1.1. Wave resources distribution

The annual mean  $H_{m0}$  and wave power generated by the wave-current coupled model are presented in Figs. 9 (a) and 10 (a). Over the ten-year period, the wave parameters display a consistent distribution pattern: values on the western side of the Orkney Islands are always higher than the eastern side, due to the North Atlantic serves as the primary source of wave energy for this region. This west-east geographic variation is most evident in the Pentland Firth. The annual mean  $H_{m0}$  and wave power at its western entrance, such as P3, reach over about 2 m and 25 kW/m, while dropping to less than about 1.25 m and 10 kW/m near Stroma Island.

Distinct inter-annual variations were observed throughout the decade. Wave height levels on the North Atlantic side were significantly higher in 2015, 2020, and 2022 compared to other years, while 2021 exhibited the lowest levels. At P2, for instance, the maximum inter-annual difference in  $H_{m0}$  was 0.5 m, dropping from 2.6 m in 2015 to 2.1 m in 2021. The variability in wave power was even greater, as summarized in Table 3. For P2, wave power ranged from a high value of 47.6 kW/m in 2015 to a low of 30.4 kW/m in 2021, a maximum inter-annual difference of 17.2 kW/m. Relative to the 10-year mean of 37.2 kW/m, this variability spanned from +28 % in 2015 to -54 % in 2021.

Similar patterns were observed at other locations. At P1, wave power variability ranged from +30 % to -20 %, and at P3, the range was +32 % to -25 %. These findings underscore the importance of long-term assessments in accurately evaluating resource potential. Reliance on data from only one or two years could lead to substantial over- or underestimation of wave energy resources.

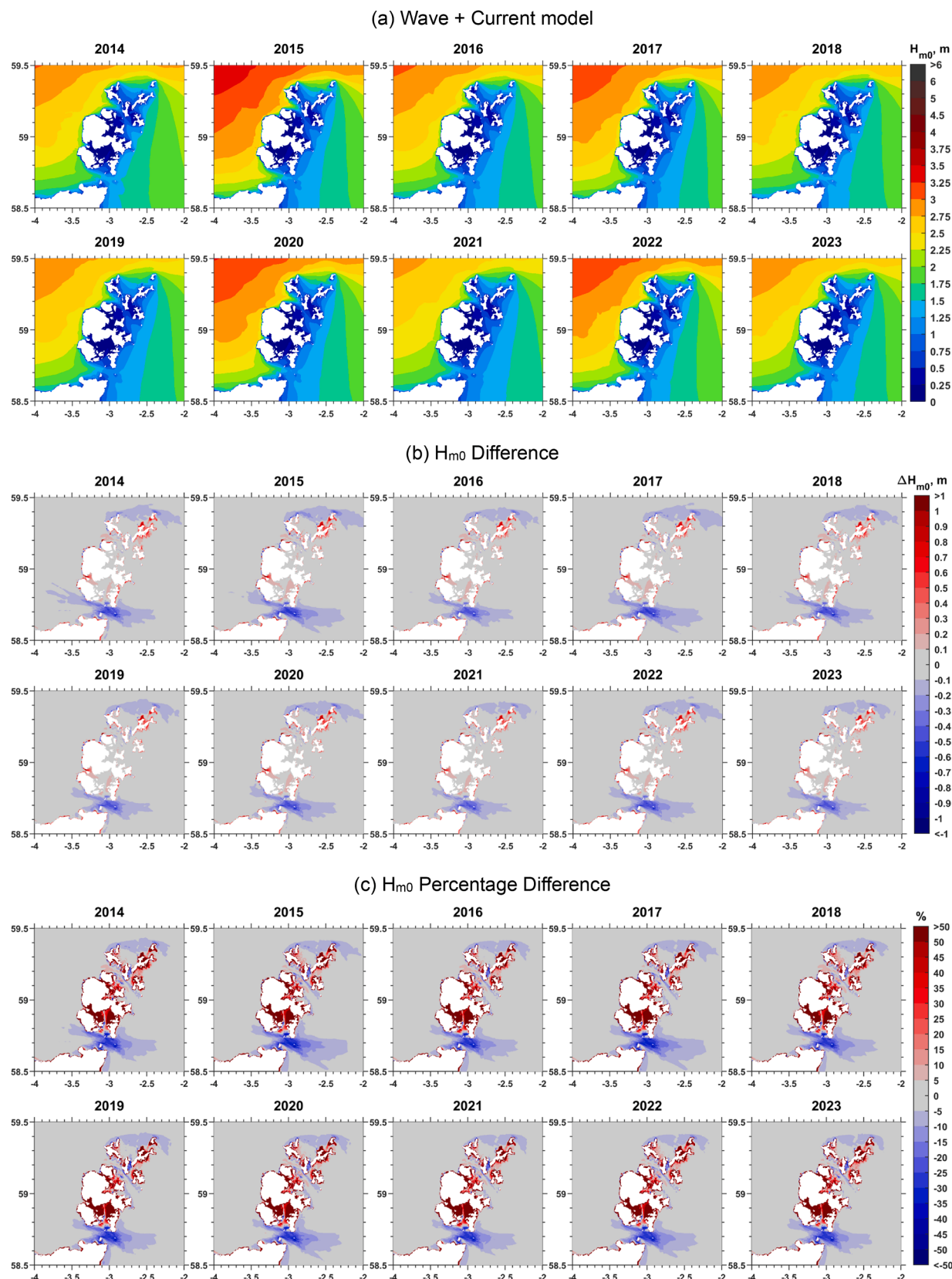


**Fig. 9.** Annual mean  $H_{m0}$  from the wave-current coupled model (a), and the differences compare to the wave-only model presented as numerical values (b) and percentages (c) for the period 2014 to 2023.

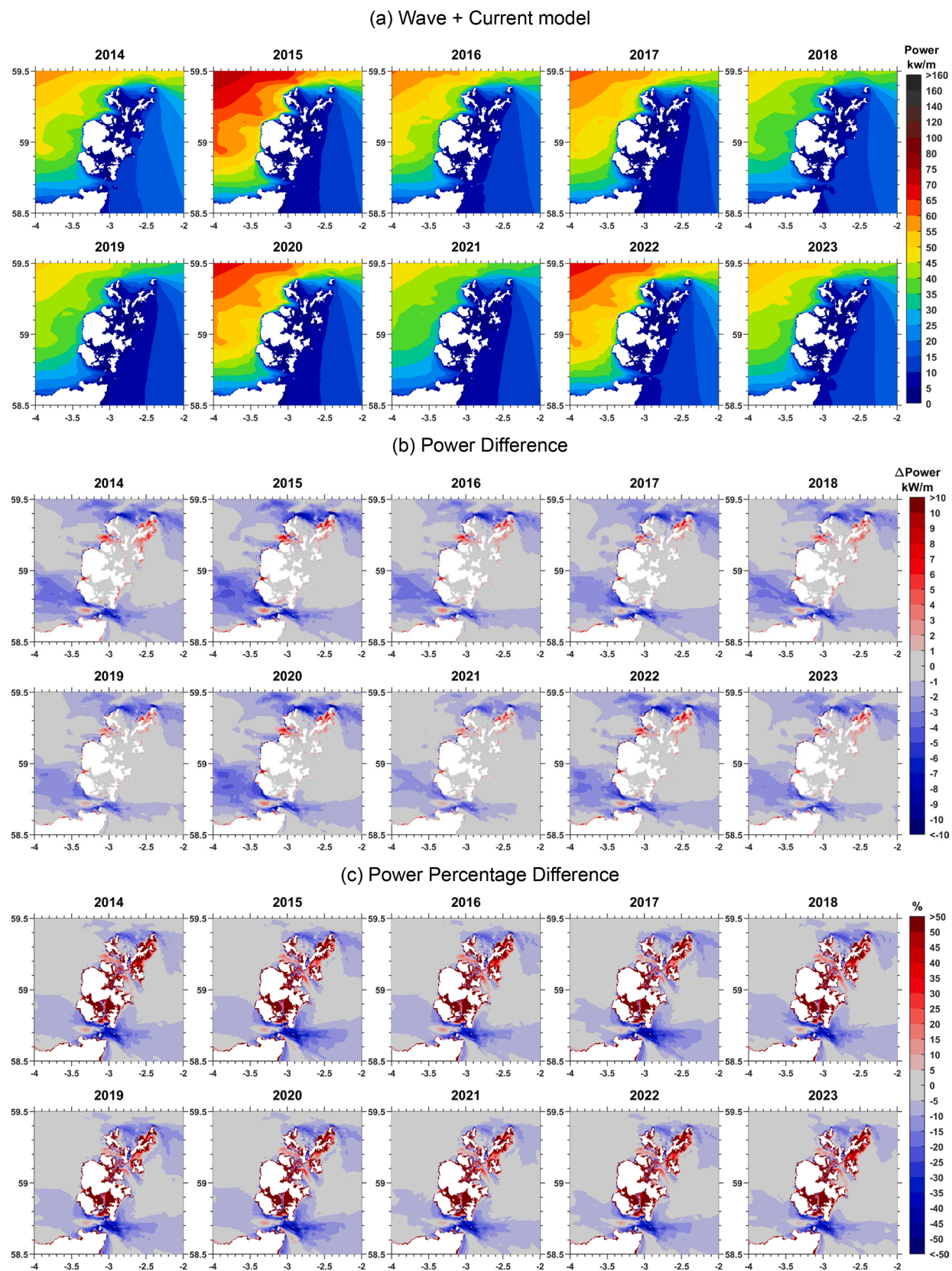


**Fig. 10.** Annual mean wave power from the wave-current coupled model (a), and the differences compared to the wave-only model presented as numerical values (b) and percentages (c) for the period 2014 to 2023.

**Table 3**

Annual mean wave power (kW/m) for the highest wave year (2015) and lowest wave year (2021), and the 10-year mean for site P1 (Westray Firth inlet), P2 (the west Orkney), and P3 (Pentland Firth inlet). “W” represents the wave-only model; “W+TC” represents the wave-current model.

Year	P1		P2		P3	
	W	W + TC	W	W + TC	W	W + TC
2015	44.3	55.0	49.8	47.6	33.4	37.6
2021	28.9	33.9	31.6	30.4	19.3	21.4
10 years mean	34.5	42.2	38.7	37.2	25.3	28.5

#### 4.1.2. North Atlantic Oscillation

The interannual variability of wave parameters can be further interpreted through the North Atlantic Oscillation (NAO) index ([http://ftp.cpc.ncep.noaa.gov/wd52dg/data/indices/nao\\_index.tim](http://ftp.cpc.ncep.noaa.gov/wd52dg/data/indices/nao_index.tim)), which is a primary driver of atmospheric circulation variability in the North Atlantic region. By calculating Pearson’s correlation coefficient between the  $H_{m0}$  at site P2 (wave-only simulation results) and the monthly NAO index (indicated by the red circle in Fig. 11 (a), a strong correlation is observed during the late winter period—January,

February, and March (JFM)—with R values exceeding 0.68. Interestingly, December shows a notably weaker correlation, with R values below 0.5, which contrasts with previous findings in (Neill and Hashemi, 2013; SP Neill et al., 2014).

To verify the consistency of this pattern, wave buoy measurements from the West of Hebrides and Blackstone stations (represented by the black and green dotted lines in Fig. 11 (a) were also examined. These independent datasets exhibit a similar result to site P2, with strong correlations during the JFM period and reduced correlation in December, thereby increasing confidence in the model results at P2. A possible explanation for the weaker correlation in December could be that it marks the onset of winter circulation, during which the NAO signal tends to be less stable and more variable. To investigate whether a lag effect might explain the discrepancy, a comparison was made for November NAO values with December wave parameters (not shown here); however, the analysis returned a negative correlation, suggesting that the weak December relationship is not due to a lagged NAO influence.

Based on these observations, the JFM period is selected for focused analysis. Figs. 11 (b) and 11 (c) present the mean  $H_{m0}$  and mean wave power for the JFM period plotted against the corresponding mean NAO

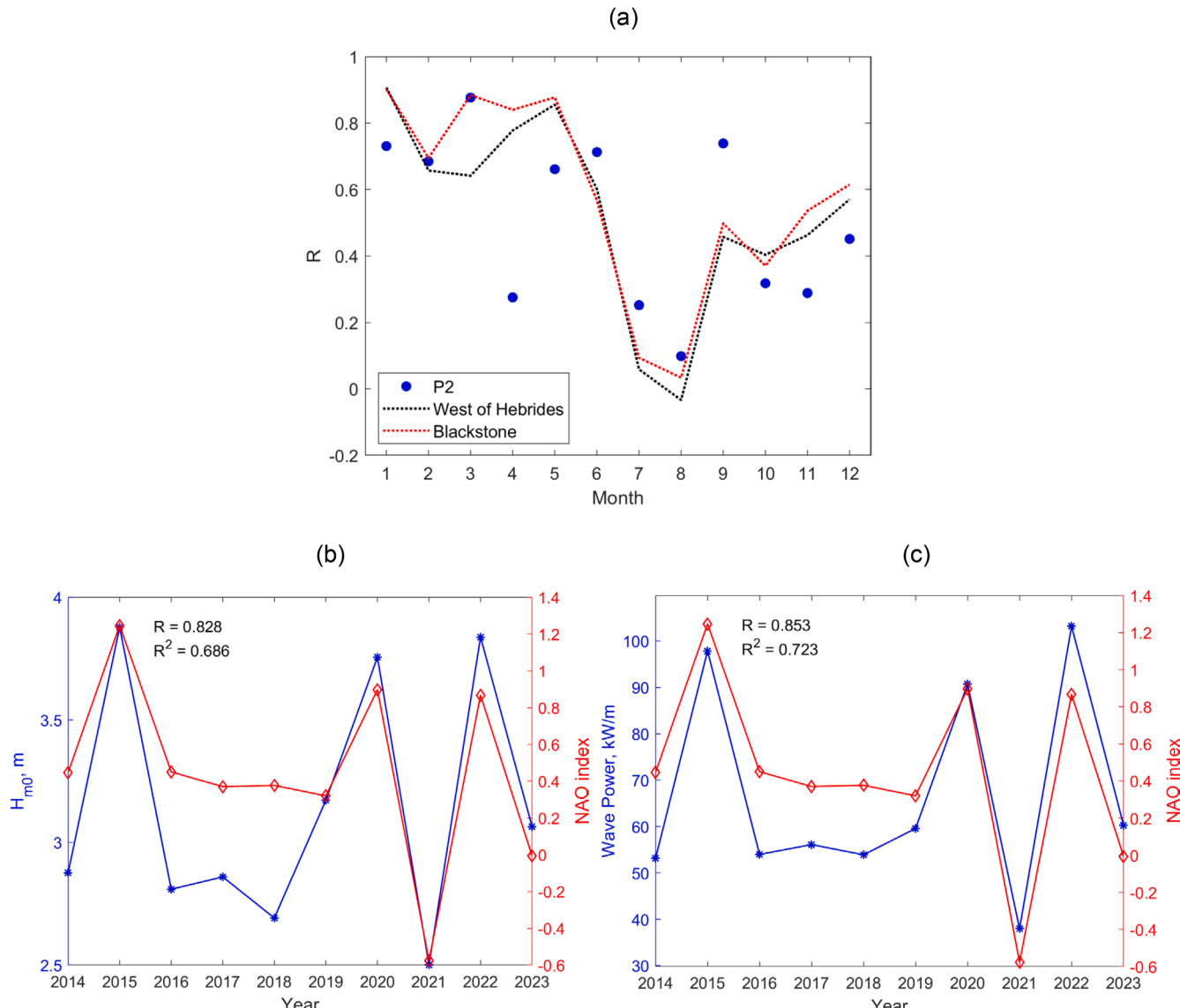


**Fig. 11.** NAO-wave relationship over 10 years. (a) Pearson's correlation coefficient between monthly  $H_{m0}$  and monthly NAO index. (b) Mean  $H_{m0}$  from JFM (January to March) at site P2 plotted against the JFM NAO. (c) Mean wave power from JFM (January to March) at site P2 against the JFM NAO.

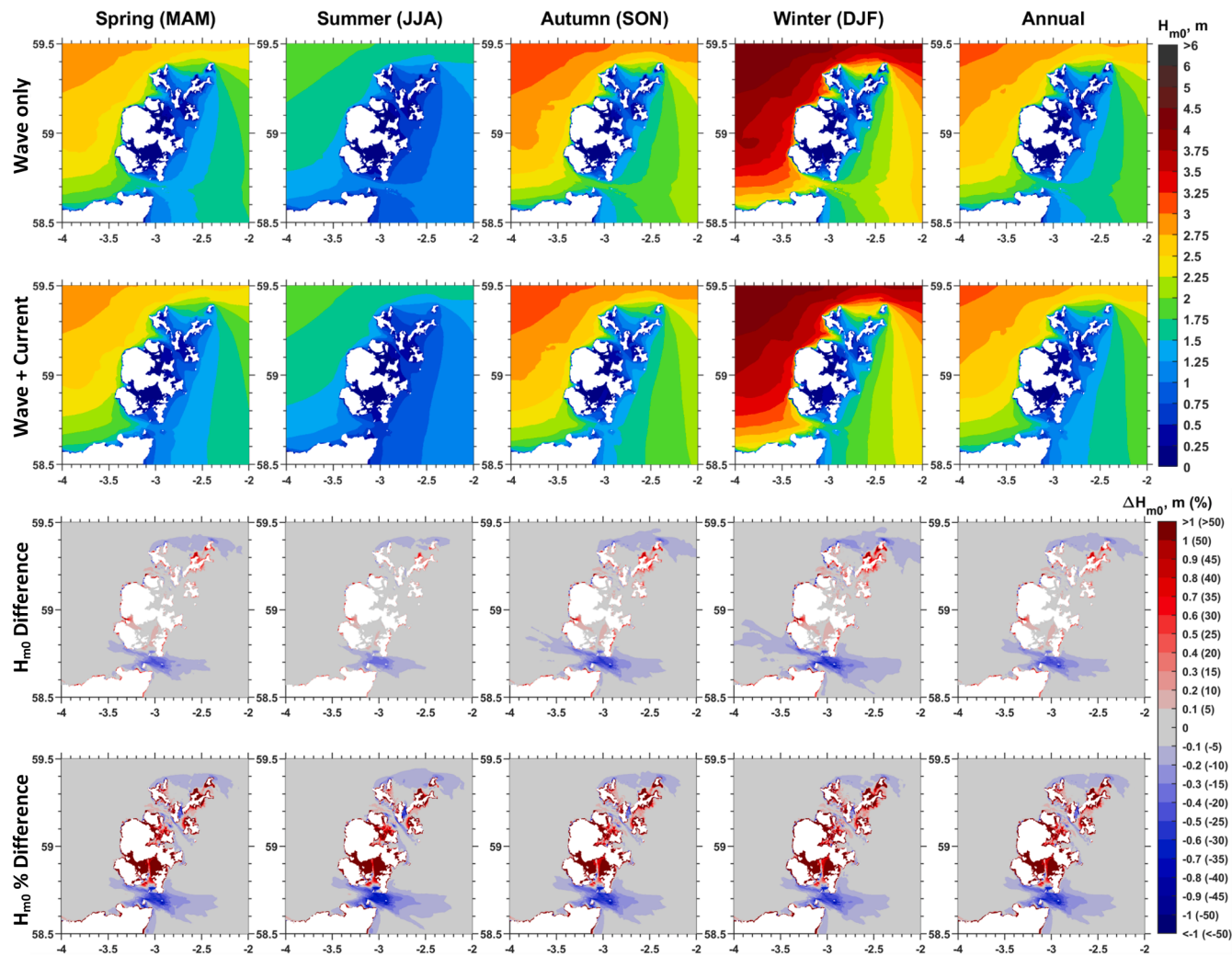


**Fig. 12.** Seasonal mean  $H_{m0}$  over 10 years from the wave-current coupled model (a), and the differences compared to the wave-only model presented as numerical values (b) and percentages (c).

index over 10 years. Both parameters show strong positive correlations with R values exceeding 0.8, indicating excellent agreement in interannual trends. Notably, the highest JFM NAO index occurred in 2015, with elevated values also seen in 2020 and 2022, while the lowest was in 2021 - findings that align well with the wave variability patterns observed in Figs. 9 and 10, as discussed earlier in this section.

#### 4.1.3. Tidal current effects

The impact of tidal currents on the wave resource is assessed by comparing simulation results from the wave-current coupled model with those from the wave-only model. Figs. 9 (b) and (c) and Figs. 10 (b) and (c) illustrate these effects for wave heights and wave power, respectively, presenting the differences (i.e., coupled model – wave model) and as percentages (i.e. (coupled model – wave model) / wave model).

**4.1.3.1. Quantification of differences between wave-only and combined wave-currents scenarios.** Minimal differences in values (indicated in grey) are observed in open sea areas, such as the northwest and eastern parts of the Orkney Islands, and in sheltered waters enclosed by islands. These regions experience weaker tidal currents, leading to negligible impacts on wave parameters. Conversely, significant differences (both in positive and negative quantities) appear in straits, tidal inlets, and along the northern and southern edges of the Orkney Islands. Here, topographic constraints accelerate tidal currents, resulting in faster flows, as shown in Fig. 8.

The reductions in wave height and wave power due to tidal currents are evident at the northern and southern edges of the Orkney Islands, including areas north of Papa Westray, North Ronaldsay, and south of the Hoy Island. However, these reductions are less severe compared to those observed around the northern and southern sides of Stroma Island in the Pentland Firth, where tidal speeds exceed 4 m/s. Here, annual wave height reduction exceeds 0.5 m, and wave power reductions surpass 6 kW/m. These overall reductions are likely driven by enhanced wave breaking of the strong tidal currents. Supporting evidence comes from time series data (Fig. 7) at the ADCP site in the Inner Sound (south of Stroma Island), which shows high-frequency, discontinuous spikes characteristic of wave-breaking events.

Conversely, tidal inlets, such as Westray Firth, Hoy Mouth and Pentland Firth, show a noticeable increase in wave power (red areas in the map). For instance, P1 and P3 exhibit annual increases of up to 9 kW/m and 4 kW/m during high-wave years (e.g., 2015, 2020, and 2022). Over the decade, the mean increase is 7.7 kW/m for P1 and 3.2 kW/m for P3, and the detailed 10-year mean annual wave power can be found in Table 3. However, changes in wave height at these regions remain minimal.

**4.1.3.2. Percentage difference.** The ‘wave height percentage difference’ map (in Fig. 9 (c)) mitigates the effects of varying wave baselines, providing a clearer representation of tidal influences. For instance, while the value difference map shows stronger tidal effects in 2015 compared

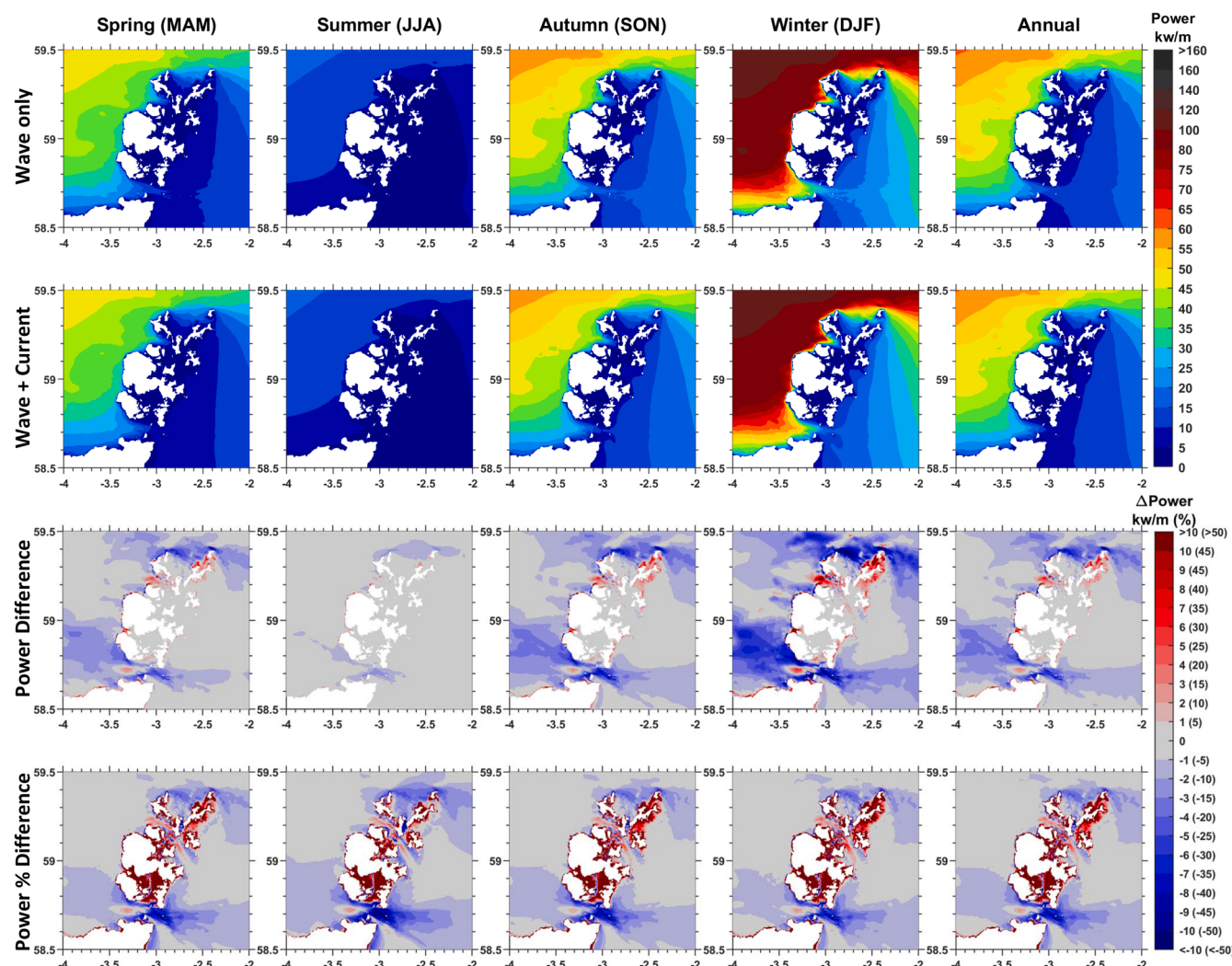


**Fig. 13.** Seasonal mean wave power over a 10-year period from the wave-current coupled model (a), and the differences compare to the wave-only model presented as numerical values (b) and percentages (c).

to 2021, the percentage difference map shows nearly identical results for both years. This consistency highlights that the influence of tidal currents remains stable over the decade, largely independent of fluctuations in wave activity. A similar pattern is evident in spatial variations: although the differences in wave power are greater in the North Atlantic compared to the North Sea, the percentage differences indicate a comparable extent of tidal influence, remaining within 10 % across both regions.

Tidal currents have their most significant influence near Stroma Island, where annual wave heights change exceeds 25 % and wave power change surpasses 50 %, far exceeding the effects seen elsewhere in the Orkney Waters. The northern and southern edges of the Orkney Islands also see the reductions, similar to the previous finding in the ‘wave

height difference’ map, with the reduced percentage in  $H_{m0}$  and wave power being over 5 % and 15 %, respectively.

In tidal inlets, wave power increases are still notable. The percentage differences of the 10-year mean wave power reach 22 % in P1 at Westray Firth and 13 % in P3 at Pentland Firth. A comparable increase is also observed in Stronsay Firth, although this effect is subtle in the numerical difference map due to the region’s low wave activity (i.e., annual mean  $H_{m0} < 1.25$  m, mean power  $< 10$  kW/m). However, percentage differences reveal the tidal effects in this tidal-active region, where maximum speeds exceed 2 m/s.

Caution is needed when interpreting changes in regions with very low wave levels (i.e.,  $H_{m0}$  closing to 0). Specifically, in enclosed waters such as Scapa Flow and coastal zones, even minor variations in wave can yield high percentage changes, appearing as dark red areas on the percentage difference map (Fig. 9 (c) and Fig. 10 (c)). However, the grey areas on the difference map indicate that tidal influence in these regions is negligible and unlikely to impact wave-current interactions meaningfully.

**Table 4**

Seasonal mean wave power (kW/m) across 10 years for site P1 (Westray Firth inlet), P2 (the west Orkney), and P3 (Pentland Firth inlet). “W” represents the wave-only model; “W+TC” represents the wave-current model.

Season	P1		P2		P3	
	W	W + TC	W	W + TC	W	W + TC
Spring	29.7	35.7	32.4	31	20.8	23.8
Summer	10.3	11.8	10.6	9.9	6.7	7.8
Autumn	34.9	41.7	38.5	36.6	25.4	28.2
Winter	63.8	80.5	74.2	71.9	48.8	54.7

#### 4.2. Inter-seasonal analysis

##### 4.2.1. Map analysis

The 10-year average wave heights and power for spring (March, April, May), summer (June, July, August), autumn (September, October,

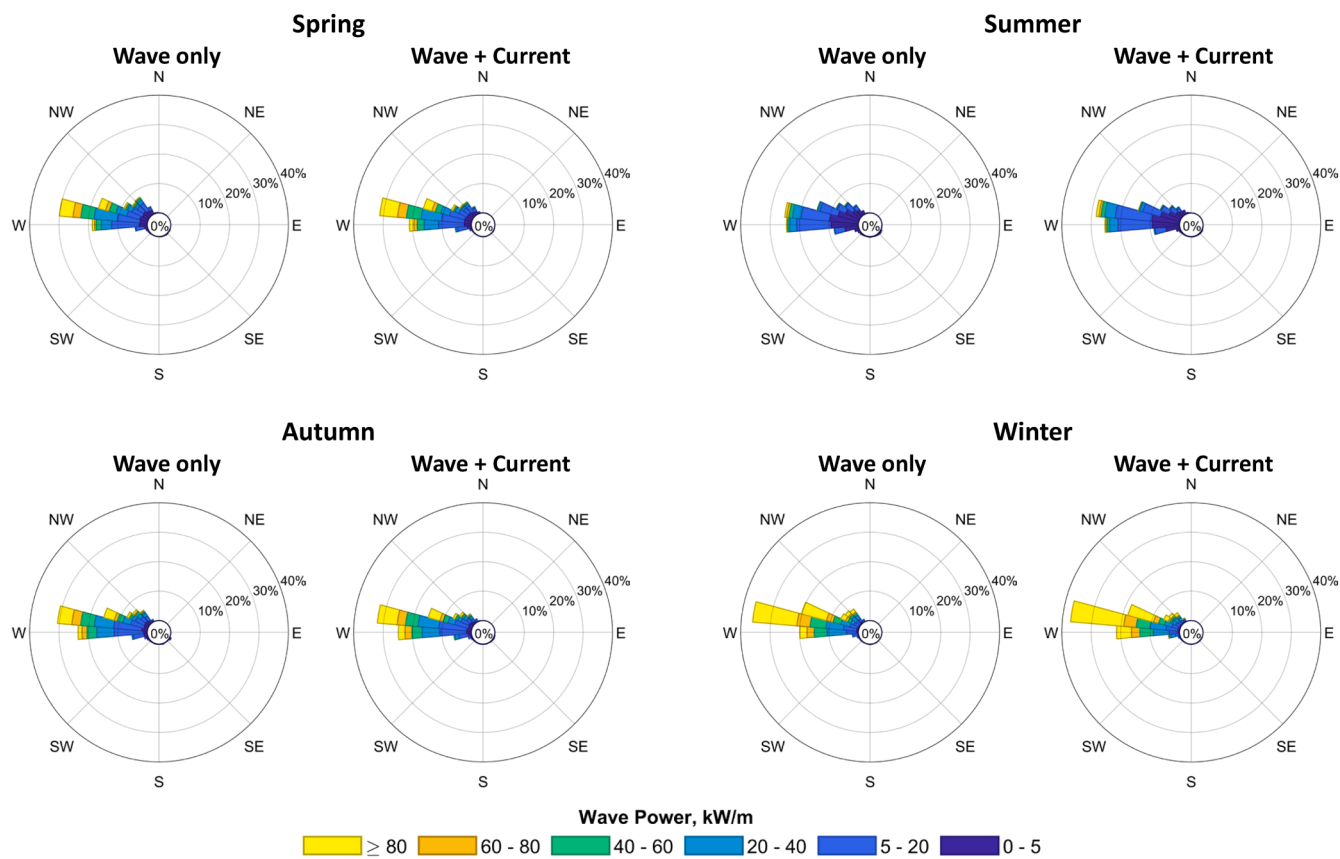


**Fig. 14.** Seasonal wave power rose plots over a 10-year period at P1 (Westray Firth inlet), comparing the wave-only model and the wave-current coupled model.

November), and winter (December, January, February) are presented in Figs. 12 and 13. These maps reveal significant seasonal variations in this region. In summer, the  $H_{m0}$  at the west Orkney nearshore areas are within 1.5 m, while it is above 3 m during the winter, with double of it in summer. This inter-season variability is more pronounced in the wave power, as summarised in Table 4. The wave-current coupled model indicates that at P1, P2, and P3, winter wave power is approximately seven times greater than in summer. Relative to the annual mean over the decade, inter-seasonal variability ranges from -72 % in summer to +91 % in winter across these sites. Interestingly, the autumn seasonal mean values at these locations are very close to the annual mean, regardless of whether tidal currents are considered. This suggests that autumn results can serve as reasonable approximations of the annual mean.

While the maps of  $H_{m0}$  and wave power do not clearly differentiate between the wave-current coupled and the wave-only models, the difference maps (by numerical values and percentages) provide further insights. Numerically, differences are smallest in summer and greatest in wave-active winters, aligning with the overall wave levels. At P1, P2, and P3, the differences in wave power during summer are 1.5 kW/m, -0.7 kW/m, and 1.1 kW/m, respectively, compared to 16.7 kW/m, -2.3 kW/m, and 5.9 kW/m in winter. Similar to the wave maps, differences in autumn closely resemble the annual differences. In contrast, percentage differences exhibit no significant seasonal variation. The regions and extents affected by tidal currents appear even slightly broader and more pronounced in summer compared to winter, highlighting the consistent nature of tidal effects irrespective of wave energy levels.

#### 4.2.2. Rose plot of wave power

To further illustrate the season variability under tidal current effects, wave power and mean wave direction are combined and presented as rose plots at P1, P2, and P3 throughout the season over the 10 years, and

are shown in Figs. 14–16. Notably, the wave directions represent the direction of ‘travel-from’; angle 0° in the rose plot points to the north, with positive values indicating clockwise rotation and bin size being 10°.

Across all sites, the primary directions contributing to wave power remain consistent across seasons, with the primary directions being around 280° for P1 and P2, and 290° for P3. As expected, winter consistently shows higher wave power. Along the primary wave directions at P1, P2, and P3, wave power exceeds 80 kW/m approximately 20 %, 15 %, and 10 % of the time during winter when tidal currents are considered.

The inclusion of tidal currents has varying effects on wave power distribution across the sites:

- P1: The distribution of wave power along the primary direction (280°) intensifies, while wave power from northern directions diminishes (i.e., angle > 280°). This suggests a more focused distribution of wave power from the west.
- P2: The main wave direction (280°) sees reduced power in the combined wave-current case, but there is an increase in wave power from the west (270°), resulting in a more dispersed distribution.
- P3: Despite an overall increase in wave power, the main wave direction (290°) experiences a power reduction, with increased contributions from westward directions (280°), which also leads to a more dispersed distribution.

For these sites, tidal currents do not drastically alter the overall distribution structure; they provide valuable insights into the potential tidal effects on wave energy resources, which could concentrate (P1) or disperse the power distribution (P2 and P3).

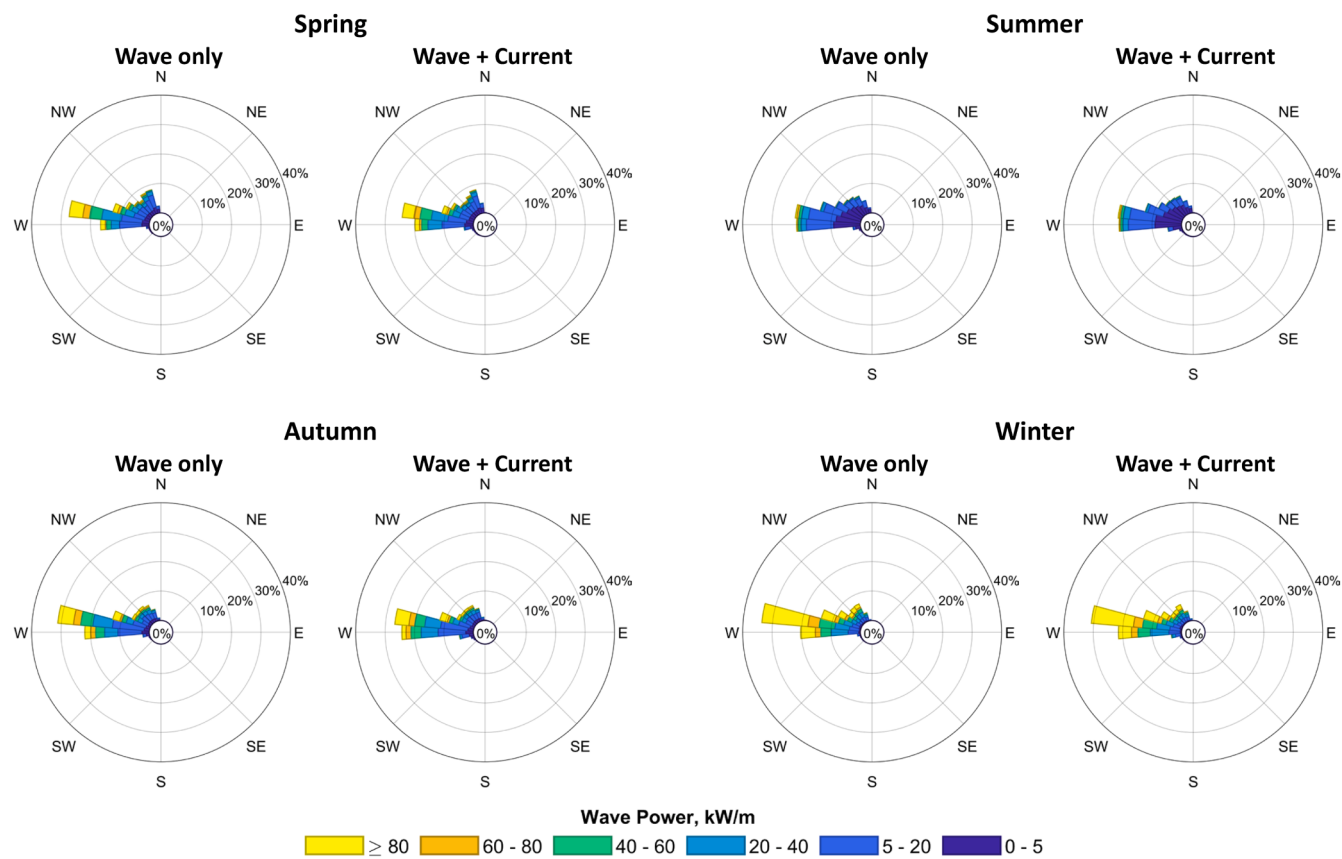


**Fig. 15.** Seasonal wave power rose plots over a 10-year period at P2 (the west Orkney), comparing the wave-only model and the wave-current coupled model.

#### 4.3. Inter-monthly analysis

##### 4.3.1. Map analysis

The monthly maps (Fig. 17) reveal that wave power is highest during the winter months, with January exhibiting the most intense wave activity. Wave power distribution in November and March is comparable, reaching up to the level of 50 kW/m at the west Orkney nearshore regions. During the transaction months between high and low wave activity, such as April and September, the monthly average wave energy power in these areas still reaches 25 kW/m. From May through August, however, the average monthly power in this area is <15 kW/m. This monthly pattern suggests that wave energy converters deployed here could benefit generation of higher energy from September to the following April, while the period from May to August might be reserved for maintenance and servicing.

According to the difference maps, the influence of tidal currents on wave energy power is most pronounced during the peak wave resource months of winter. For example, in January, a reduction in wave energy exceeding 10 kW/m was observed around Stroma Island, as well as in the southern and northern edges of the Orkney Islands (i.e., south of the Hoy Island, north of Papa Westray and North Rondalsay). In contrast, an increase in wave power, with values rising above 10 kW/m and 7 kW/m, was observed at the tidal entrances of Westray Firth and Pentland Firth, respectively.

##### 4.3.2. Box plot analysis

Fig. 18 presents the 10-year annual cycle of wave power for each month at P1, P2, and P3 using box plots, where the median (middle marker) is used as a representative value. The box's upper and lower edges represent the 75th and 25th percentiles, respectively. Every box covers 50 % of the data range around their median and providing a clear depiction of typical monthly wave power variations.

The box plots confirm that January has the strongest wave power overall, including the highest maximum values (upper edge), the widest data range, and the largest median values. In contrast, July shows the weakest wave power. As summarized in Table 5, the median wave power across these three sites in July is <10 % of the January value.

Including tidal currents in the simulations has varying effects at these locations:

- For P1 and P3, tidal currents increase overall wave power levels by resulting in higher maximum and median values and causing greater data variability each month. For example, in January, median values increase by 12 % (from 54.5 to 62 kW/m at P1 and 31.4 to 35.3 kW/m at P3). The data range (25th to 75th percentiles) widens by 23 % at P1 and 10 % at P3.
- For P2, tidal currents result in a more concentrated power distribution, with slightly reduced maximum values and narrower variability. The median decreases by 6 %, and the interquartile range narrows by 3 %.

While the increased median values at P1 and P3 highlight greater potential for wave energy development, the accompanying increase in power variability may pose challenges for stable power output and device survivability. Conversely, the concentration of power variability at P2 reduces overall power output, making it less favourable. An ideal WEC site would exhibit minimal tidal effects, stable power variability, and consistent energy output.

It is important to note that the maximum values in the box plots exclude outliers and may not represent the 10-year extreme values discussed in subsequent sections.

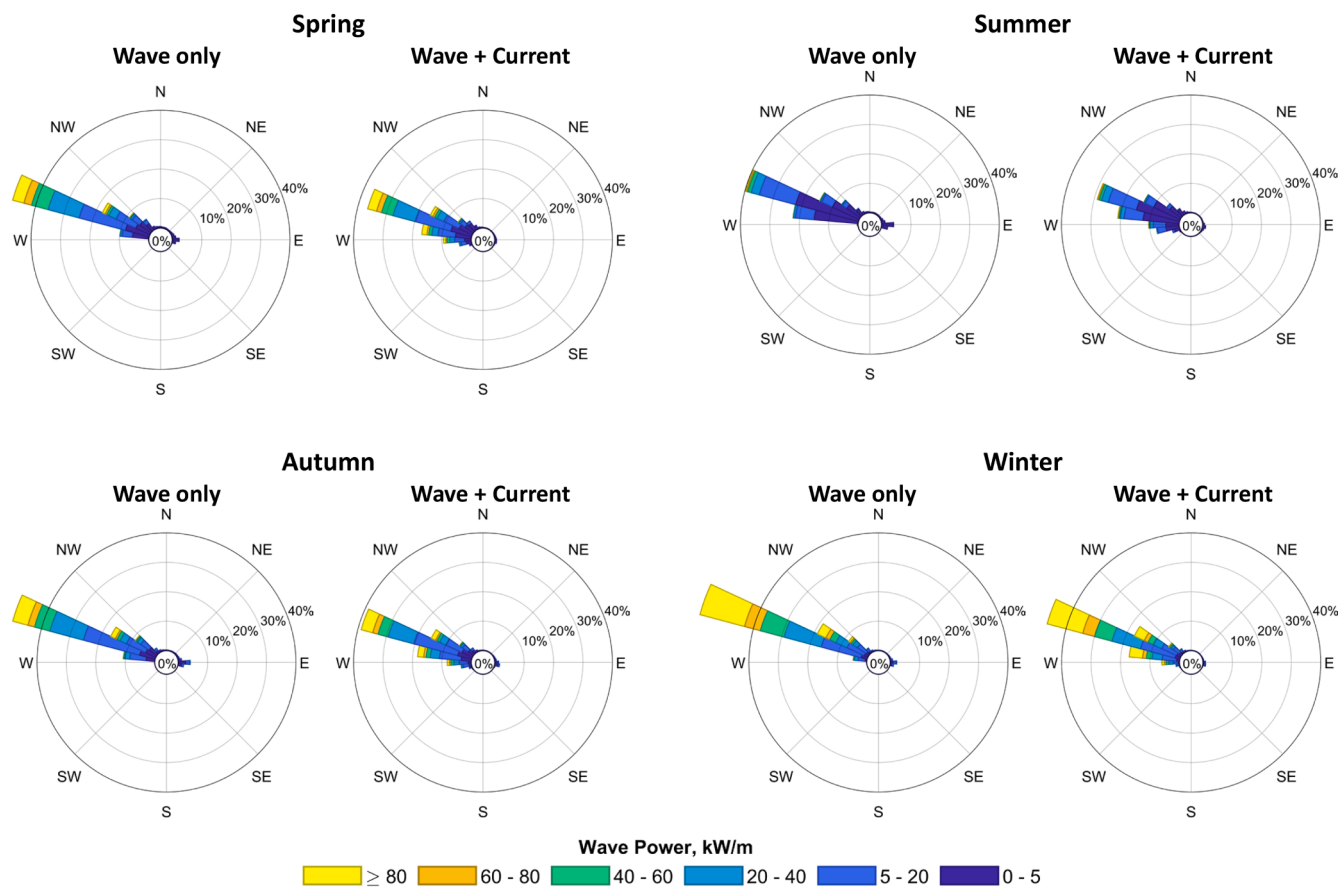


**Fig. 16.** Seasonal wave power rose plots over a 10-year period at P3 (Pentland Firth inlet), comparing the wave-only model and the wave-current coupled model.

#### 4.4. Ten years extreme

This section examines the extreme wave height and wave power in the Orkney waters over a decade, as predicted by the wave-only model, the wave-current coupled model, and their differences, as shown in Fig. 19. These maps are critical for informing the design of WECs to ensure stability and survivability under extreme conditions.

Unlike the predominantly blue colour of the previous difference maps (i.e., Fig. 9 (b) (c), Fig. 10 (b) (c), lower two rows of Fig. 12 and Figs. 13, and Fig. 17 (b)), the extreme value difference maps are dominated by red colour, indicating that tidal currents amplify extreme sea states. For instance, at P2, where mean and median wave parameters previously showed a decrease due to tidal currents, the inclusion of tidal effects raises extreme wave heights from 9.2 m to 9.4 m and extreme wave power from 551.6 kW/m to 577.4 kW/m.

This increase is unsurprising and most significant at the tidal inlets. At P1, extreme wave height rises from 5.7 m to 7.8 m (over a 2 m increase), and wave power increases from 242 kW/m to 469 kW/m (a net increase of 227 kW/m). At P3, extreme wave height increases from 8.7 m to 10.1 m (1.4 m increase), and wave power rises from 460.2 kW/m to 687.4 kW/m (a net increase of 227.2 kW/m).

It is important to note that numerical models tend to underestimate extreme values, as observed in the model validation, where peak values were consistently underpredicted. Therefore, the actual extreme wave conditions in reality are likely to exceed the values reported in this study. These findings underscore the significant role of tidal currents in intensifying extreme sea states and highlight the importance of accounting for wave-current interactions in the design and operation of marine energy infrastructure.

#### 5. Limitations and further thoughts

##### 5.1. Model limitations

The coupled wave-current numerical model applied in this study uses constant parameters across the entire simulation domain of the regional model, such as the bottom friction coefficient in the flow model and the dissipation coefficient for strong currents in the wave model. While these parameters are effective on a broad scale, they may not be optimal for specific areas within the domain, potentially leading to inaccuracies in tidal current or wave predictions at certain locations. This limitation is particularly relevant given the large area of the regional model, as shown in the bathymetry in Fig. 2, where shallow regions with depths under 20 m may exhibit greater variability in representation.

Such concerns are not unique to this study and are common in numerical modelling. It is impractical to ensure that all areas are perfectly simulated, especially in large domains. To address this, validation over extended periods is critical. In this study, the model was validated over a total of 135 days, covering both summer and winter, at two locations situated in dynamic wave-current environments: Westray Firth and Pentland Firth. These locations are geographically distant and present significant tidal complexities, yet the model achieved robust validation results, demonstrating its reliability in this region with water depth deeper than 30 m.

However, inaccuracies in the coastal regions of the coupled model are acknowledged, such as the west Orkney coastlines shown in the difference map by numerical values. This is particularly relevant in areas where water levels may intermittently drop to zero or below, forcing the model to simulate unrealistic coupling processes. For research focused on specific coastal zones, higher-resolution models would be necessary.

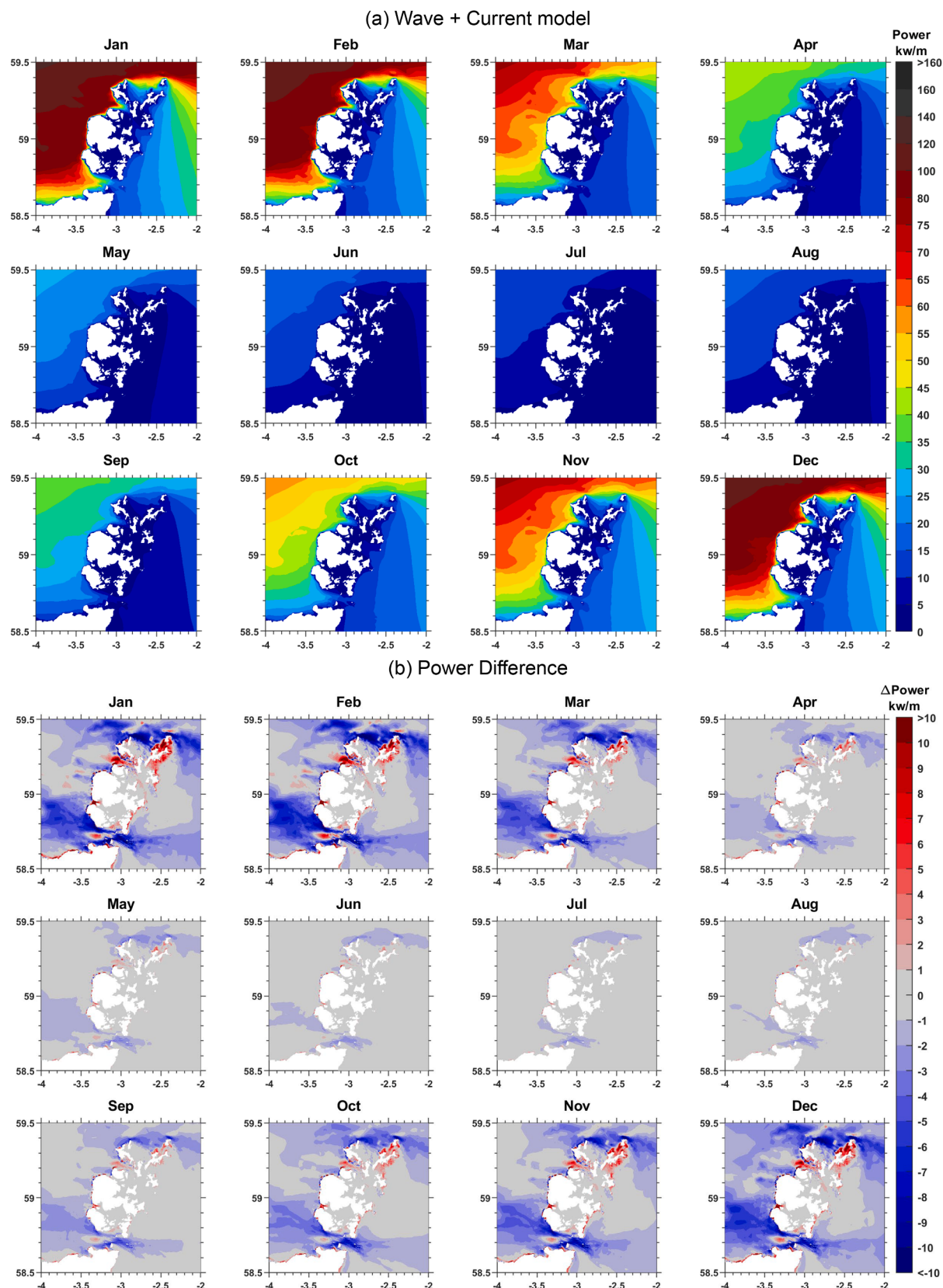


**Fig. 17.** Monthly mean wave power over a 10-year period from the wave-current coupled model (a) and the differences compared to the wave-only model presented as numerical values (b).

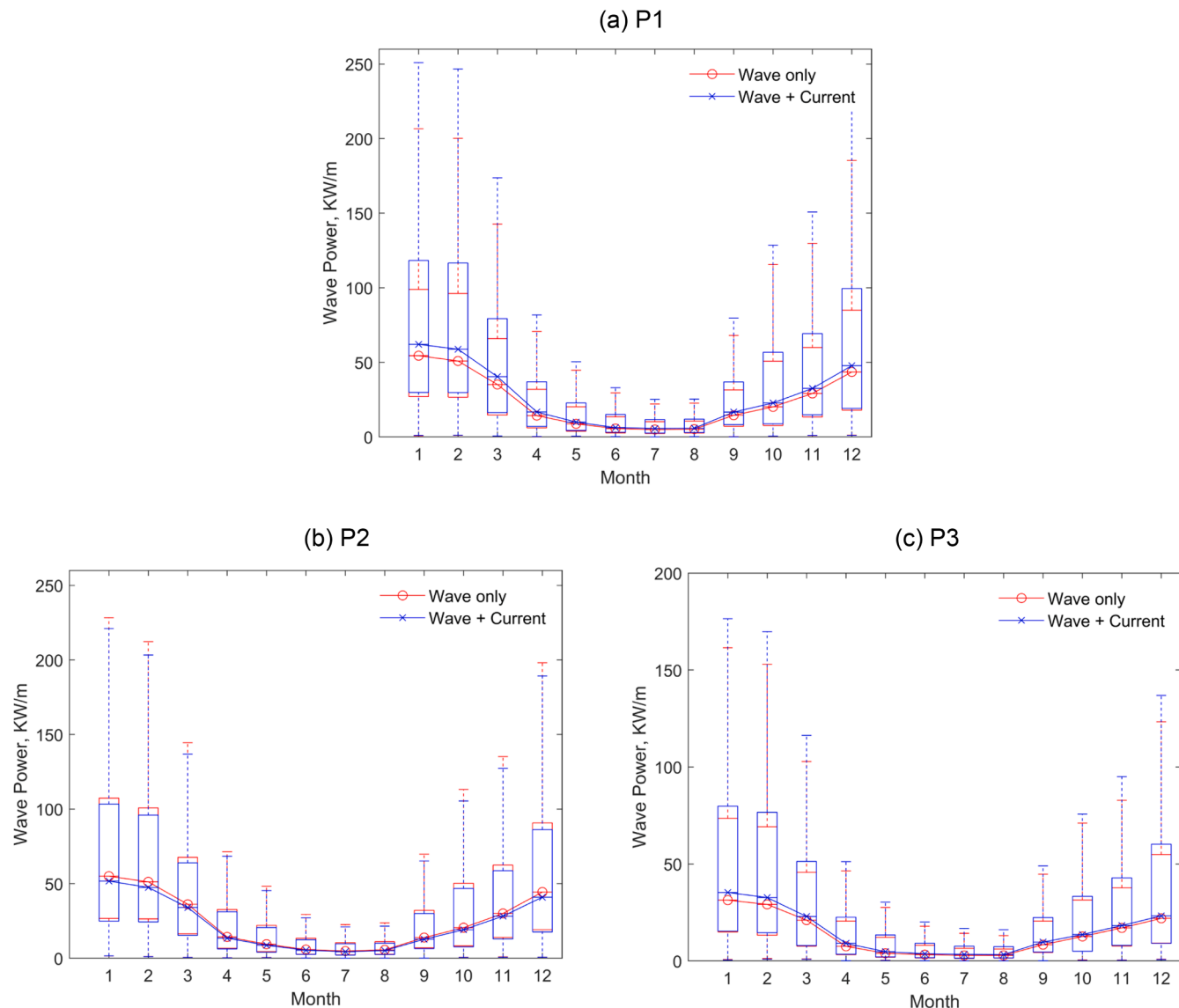


**Fig. 18.** Boxplots of the annual cycles of the wave power of every month across 10 years, for site P1 (Westray Firth inlet), P2 (the west Orkney), and P3 (Pentland Firth inlet).

**Table 5**

Data features of the wave power (kW/m) for January and July across 10 years for site P1 (Westray Firth inlet), P2 (the west Orkney), and P3 (Pentland Firth inlet). “W” represents the wave-only model; “W+TC” represents the wave-current model. The ‘75 % - 25 %’ rows represent the interquartile range (IQR), calculated as the difference between the 75th and 25th percentiles of the data.

Month	Feature	P1		P2		P3	
		W	W + TC	W	W + TC	W	W + TC
January	Median	54.5	62.0	55.0	51.7	31.4	35.3
	75 % - 25 %	71.9	88.5	80.7	78.5	58.2	64.4
July	Median	4.9	5.7	4.8	4.4	2.8	3.4
	75 % - 25 %	7.6	9.0	8.3	7.6	5.1	6.2

Additionally, the 10-year simulation was conducted by running 20 numbers of 6-month simulations and combining the results. For each simulation, the initial two days were excluded from analysis due to potential spin-up effects. Given the long-term statistical nature of this study, the exclusion of these brief periods does not significantly impact the overall results.

Furthermore, the high density of contours on the maps may create a visual impression of elevated values in certain regions, making them appear more intense than they actually are. For accurate analysis, results should be interpreted based on the actual data values rather than relying solely on visual intensity.

This study focuses only on wave resource assessment impacted by wave-current interactions. As the wave model used for this study was a phase resolved model, the changes to the waves and tidal currents in time-domain as wave-by-wave cycles, are not possible. If one is interested in estimating tidal energy resource with the inclusion of wave-current interactions, the contour maps presented in Fig. 8 could easily be used to obtain tidal energy corresponding to different phases of the tide.

## 5.2. A comparison to the previous long-term study for Orkney Waters

This study extends the work of Neill et.al in 2014 (Neill et al., 2014), who used the SWAN spectral wave model to produce a 10-year wave parameter dataset for the Orkney Waters, spanning 2005–2014. Their research provided a valuable foundation for assessing long-term inter-annual and inter-seasonal wave energy resources in the region.

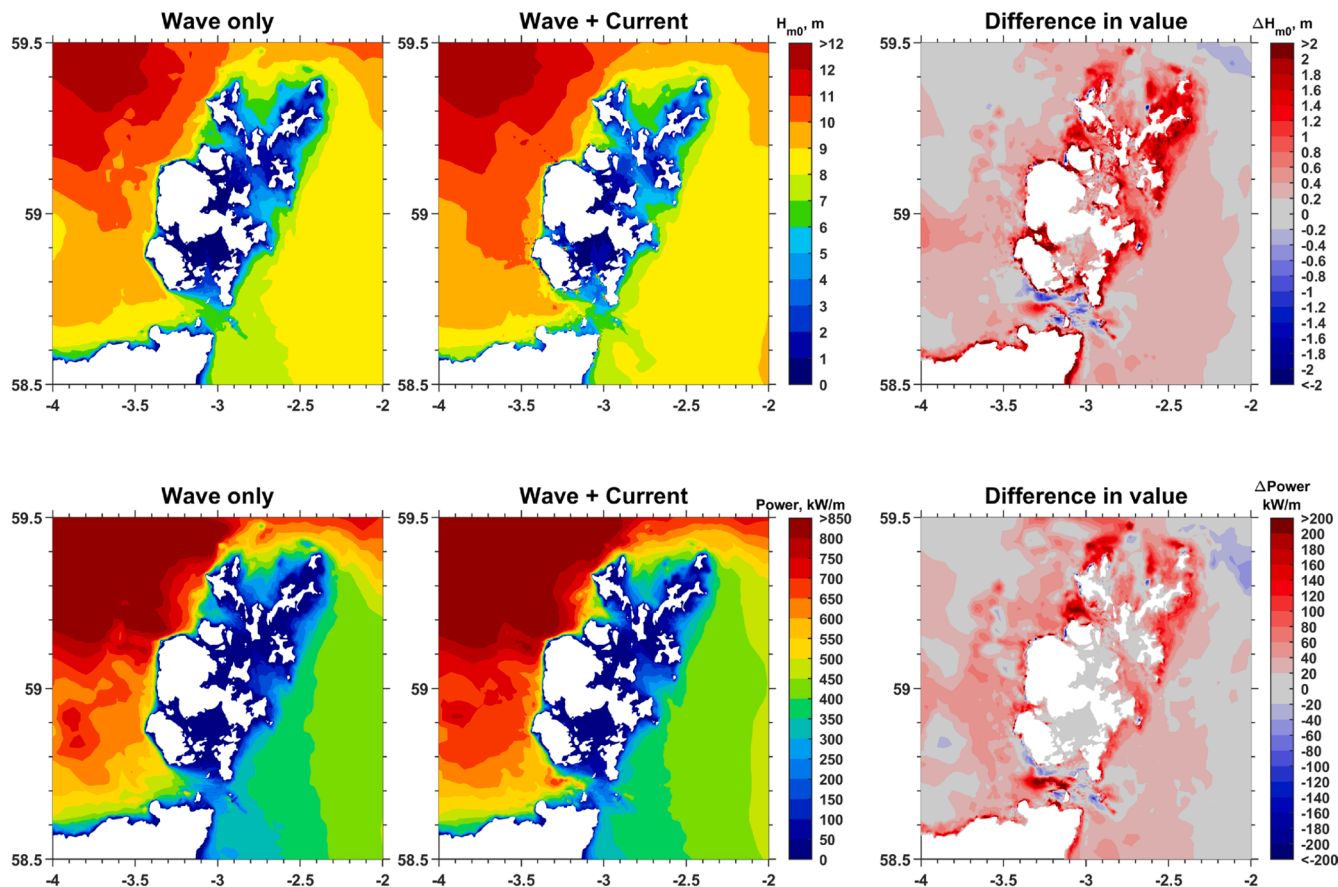


**Fig. 19.** Maximum  $H_{m0}$  (upper plots) and wave power (lower plots) over a 10-year period from the wave-only and wave-current coupled model, with differences presented as numerical values.

However, their results appear to underestimate wave power compared to those presented here.

Evidence to support this is that the annual mean wave power estimated by the MIKE21 in 2012 (Venugopal and Nemalidinne, 2015) is significantly higher than the mean wave power calculated by Neill et al. during the extended winter season (December–March) in the same year, which is unrealistic. The inter-annual validation of the SWAN model is mainly proved by the Pearson correlation coefficient R with the North Atlantic Oscillation (NAO) index. It is acknowledged that the NAO index serves as an important reference for long-term ocean modelling (Mackay et al., 2010), while it mainly focused on the trend rather than the value. High correlation with the NAO index does not necessarily ensure accurate value predictions. A potential reason for the underestimation of wave power in the SWAN model lies in its default wave power calculation method, which can lead to underestimations of up to 15 %, as observed in the Sea of Iroise when compared to TOMAWAC (Guillou, 2015).

In contrast, this study conducted continuous validation using 10 years of wave buoy measurements across four different locations. The consistent agreement between the model results and field data provides confidence not only in the trend (e.g., R) but also in the accuracy of the absolute values of the simulation results (e.g., Bias, RMSE, and SI). This robustness strengthens the case for using the TOMAWAC-TELEMAC coupled model for long-term wave energy resource assessments in regions with significant wave-current interactions.

## 6. Conclusion

This study employed a North Atlantic scale wave-only model, and a regional scale coupled wave-current model to conduct a 10-year

(2014–2023) hindcast simulation. This approach provided accurate interannual, seasonal, and monthly wave data for Orkney Waters and Pentland Firth, including tidal effects, thus revealing the long-term influence of wave-current interactions. The feasibility of this research relies on the TOMAWAC spectral wave model and TELEMAC flow model, both sub-modules of the open-source Telemac system, which enable a straightforward two-way coupling process between waves and tidal currents.

The interannual reliability of the model was confirmed through 10-year time-series validation with wave buoy measurements at four locations and further supported by correlation with the North Atlantic Oscillation index. The effectiveness of the wave-current coupled model was demonstrated by a 135-day comparison with AWAC and ADCP data, both deployed in environments with coexisting waves and currents. With these validated techniques, key findings from this study include:

- 1. Wave Resource Variability:** Significant interannual, seasonal, and monthly variability was observed in the wave resources around Orkney. For example, at P2, a site located on the west of Orkney Mainland, the wave power in a wave-active year (2015) is 47.6 kW/m and in a wave-weak year (2021) is 30.4 kW/m. Compared to its 10-year mean result, this variability ranged from +28 % to -25 %. Seasonal variability in wave power ranges from -72 % in summer to +91 % in winter across the sites of P1, P2, and P3, compared to their annual mean results. The inter-monthly variability is more significant, with the median power production in July being just 10 % of that in January across all sites.
- 2. Tidal Effects on Wave Reduction:** When tidal currents are considered, wave height and wave power significantly decrease along the northern and southern edges of the Orkney Islands, and

- along the northern and southern edges of Stroma Island in Pentland Firth. The decrease is most substantial at the latter one, with an annual decrease in  $H_{m0}$  and wave power of over 0.5 m (change by over 25 %) and 6 kW/m (over 50 %).
3. **Tidal Effects on Wave Increase:** At the central mouths of tidal inlets (Westray Firth, Hoy Mouth, and Pentland Firth), wave power generally rises when tidal effects are included. For instance, the annual mean wave power at P1 in Westray Firth inlet and P3 in Pentland Firth inlet reaches up to 7.7 kW/m (22 % increase) and 3.2 kW/m (13 % increase) over the decade. The increase phenomenon is always more obvious in wave power than in wave heights.
  4. **Wave-Current Interactions Variability:** The numerical difference between the wave-only and wave-current coupled models varies significantly by year, season, and month, following a general concept that the period of higher wave levels leads to a higher value difference. In contrast, the percentage difference map remains relatively steady across different times, highlighting the consistent nature of tidal effects relatively irrespective of wave levels.
  5. **Extreme Wave Values with Tidal Effects:** Tidal currents always amplify the extreme conditions of the sea states. At the P1 and P3, the tidal currents amplify the wave heights by 2 m and 1.4 m higher to become 7.8 m and 10.1 m, and the wave power around 227 kW/m higher than before to be 469 and 687.4 kW/m, respectively.

The results presented in this research provide a high level of confidence for wave hindcasting in the Pentland Firth and Orkney Waters, with natural tidal current effects inherently incorporated. The high-resolution, 10-year dataset, featuring 10-minute time intervals, offers a robust foundation for future machine learning applications in ocean science and engineering.

## Author statements

- We, the authors, confirm the following:
- Originality:** The work described in this manuscript is original and has not been published previously, nor is it under consideration for publication elsewhere, in whole or in part.

## Ethics approval

- Not applicable.
- All authors have read and approved the final version of the manuscript and agree with its submission to Applied Ocean Research.

## CRediT authorship contribution statement

- Tian Tan:** Writing – review & editing, Writing – original draft, Validation, Software, Resources, Methodology, Formal analysis, Data curation. **Vengatesan Venugopal:** Writing – review & editing, Visualization, Supervision, Resources, Project administration, Methodology, Investigation, Funding acquisition, Conceptualization.

## Declaration of competing interest

- The authors declare the following financial interests/personal relationships which may be considered as potential competing interests:

Vengatesan Venugopal reports financial support was provided by The University of Edinburgh. If there are other authors, they declare that they have no known competing financial interests or personal relationships that could have appeared to influence the work reported in this paper.

## Data availability

All simulation results generated from the numerical models developed in this study, including the North Atlantic wave-only model and

the Pentland Firth and Orkney Waters regional-scale wave–current coupled model, are available from the corresponding author upon reasonable request.

## Acknowledgements

The authors acknowledge support from the SAE MeyGen project for providing ADCP data. The authors are grateful for financial support from the UK Engineering and Physical Sciences Research Council through CableDyn: Subsea Power Cable Dynamics Under Complex Ocean Environment (EP/W015102/1).

## References

- Abdul Rahman A, Venugopal V. Inter-comparison of 3D tidal flow models applied to Orkney Islands and Pentland Firth, 2015.
- Awk, T., 2019a. TOMAWAC user manual version 8.1. The TELEMAC-Mascaret Consortium 7.
- Awk, T., 2019b. TELEMAC 3D user manual version 8.1. The TELEMAC-Mascaret Consortium 7.
- AWS Ocean Energy: EMEC: European Marine Energy Centre n.d. <https://www.emec.org.uk/about-us/wave-clients/aws-ocean-energy/> (accessed July 13, 2024).
- Barbariol, F., Benetazzo, A., Carniel, S., Sclavo, M., 2013. Improving the assessment of wave energy resources by means of coupled wave-ocean numerical modeling. Renew. Energy 60, 462–471. <https://doi.org/10.1016/j.renene.2013.05.043>.
- Benetazzo, A., Carniel, S., Sclavo, M., Bergamasco, A., 2013. Wave-current interaction: effect on the wave field in a semi-enclosed basin. Ocean. Model. (Oxf) 70, 152–165. <https://doi.org/10.1016/j.ocemod.2012.12.009>.
- Bertotti, L., Cavalieri, L., 2012. Modelling waves at Orkney coastal locations. J. Marine Syst. 96–97, 116–121. <https://doi.org/10.1016/j.jmarsys.2012.02.012>.
- Booij N, Holthuijsen LH, Ris RC. The “swan” wave model for shallow water 2015: 668–76. <https://doi.org/10.1061/9780784402429.053>.
- Cefas - WaveNet interactive map n.d. <https://wavenet.cefas.co.uk/Map> (accessed May 10, 2023).
- Coles, D., Greenwood, C., Vogler, A., Walsh, T., Taaffe, D., 2018. Assessment of the turbulent flow upstream of the Meygen Phase 1A tidal stream turbines. In: Proceedings of the Asian Wave and Tidal Energy Conference. Taipei, Taiwan, pp. 9–13.
- Copernicus Climate Change Service (C3S). ERA5: fifth generation of ECMWF atmospheric reanalyses of the Global Climate Copernicus Climate Change Service Climate Data Store (CDS) 2017. [https://cds.climate.copernicus.eu/cdsapp#!/home](https://cds.climate.copernicus.eu/cdsapp#!/) (accessed August 17, 2022).
- CorPower Ocean: EMEC: European Marine Energy Centre n.d. <https://www.emec.org.uk/about-us/wave-clients/corpowers-ocean/> (accessed December 2, 2024).
- DHI, 2024. MIKE 21/3 | 2D, 3D, Marine Water Modelling Software. DHI. <https://www.dhigroup.com/technologies/mikepoweredbydhi/mike-21-3>. accessed July 14, 2024.
- Dodet, G., Bertin, X., Bruneau, N., Fortunato, A.B., Nahon, A., Roland, A., 2013. Wave-current interactions in a wave-dominated tidal inlet. J. Geophys. Res.: Oceans 118, 1587–1605. <https://doi.org/10.1002/jgrc.20146>.
- Egbert, G.D., Erofeeva, S.Y., 2002. Efficient inverse modeling of barotropic ocean tides. J. Atmos. Ocean. Technol. 19, 183–204. [https://doi.org/10.1175/1520-0426\(2002\)019<0183:EIMBO>2.0.CO;2](https://doi.org/10.1175/1520-0426(2002)019<0183:EIMBO>2.0.CO;2).
- Gleizon, P., Murray, A., 2014. Modelling Wave Energy in Archipelagos. Case of Northern Scotland.
- Gleizon, P., Woolf, D., 2013. Wave energy assessment in Scottish Seas. In: Proceedings of the 10th European Wave and Tidal Energy Conference. Aalborg, Denmark.
- Grid-connected wave test site : EMEC: European Marine Energy Centre n.d. <https://www.emec.org.uk/facilities/wave-test-site> (accessed July 13, 2024).
- Group TW. The WAM model—A third generation ocean wave prediction model 1988.
- Guillou, N., 2015. Evaluation of wave energy potential in the Sea of Iroise with two spectral models. Ocean Eng. 106, 141–151. <https://doi.org/10.1016/j.oceaneng.2015.06.033>.
- Guillou, N., 2017. Modelling effects of tidal currents on waves at a tidal stream energy site. Renew. Energy 114, 180–190. <https://doi.org/10.1016/j.renene.2016.12.031>.
- Hopkins, J., Elgar, S., Raubenheimer, B., 2016. Observations and model simulations of wave-current interaction on the inner shelf. J. Geophys. Res.: Oceans 121, 198–208. <https://doi.org/10.1002/2015JC010788>.
- Laminaria: EMEC: European Marine Energy Centre n.d. <https://www.emec.org.uk/about-us/wave-clients/laminaria/> (accessed July 13, 2024).
- Lavidas, G., Venugopal, V., Friedrich, D., 2017. Wave energy extraction in Scotland through an improved nearshore wave atlas. Int. J. Marine Energy 17, 64–83. <https://doi.org/10.1016/j.ijome.2017.01.008>.
- Lewis, M., Neill, S.P., Robins, P., Hasheemi, M.R., Ward, S., 2017. Characteristics of the velocity profile at tidal-stream energy sites. Renew. Energy 114, 258–272. <https://doi.org/10.1016/j.renene.2017.03.096>.
- Mackay, E.B.L., Bahaj, A.S., Challenor, P.G., 2010. Uncertainty in wave energy resource assessment. Part 2: variability and predictability. Renew. Energy 35, 1809–1819. <https://doi.org/10.1016/j.renene.2009.10.027>.
- Mocean Energy: EMEC: European Marine Energy Centre n.d. <https://www.emec.org.uk/about-us/wave-clients/mocean-energy/> (accessed July 19, 2024).

- Neill, S.P., Hashemi, M.R., 2013. Wave power variability over the northwest European shelf seas. *Appl. Energy* 106, 31–46. <https://doi.org/10.1016/j.apenergy.2013.01.026>.
- Neill, S.P., Hashemi, M.R., Lewis, M.J., 2014a. The role of tidal asymmetry in characterizing the tidal energy resource of Orkney. *Renew. Energy* 68, 337–350. <https://doi.org/10.1016/j.renene.2014.01.052>.
- Neill, S.P., Lewis, M.J., Hashemi, M.R., Slater, E., Lawrence, J., Spall, S.A., 2014b. Inter-annual and inter-seasonal variability of the Orkney wave power resource. *Appl. Energy* 132, 339–348. <https://doi.org/10.1016/j.apenergy.2014.07.023>.
- Neill, S.P., Vögler, A., Goward-Brown, A.J., Baston, S., Lewis, M.J., Gillibrand, P.A., et al., 2017. The wave and tidal resource of Scotland. *Renew. Energy* 114, 3–17. <https://doi.org/10.1016/j.renene.2017.03.027>.
- Perez Ortiz A. A systematic approach to undertake tidal energy resource assessment with Telemac-2D 2013.
- Saruwatari, A., Ingram, D.M., Cradden, L., 2013. Wave-current interaction effects on marine energy converters. *Ocean Eng.* 73, 106–118. <https://doi.org/10.1016/j.oceaneng.2013.09.002>.
- Scale test sites: EMEC: European Marine Energy Centre n.d. <https://www.emec.org.uk/facilities/scale-test-sites/> (accessed July 13, 2024).
- Tan, T., Venugopal, V., 2023. Numerical modelling of wave and tidal current interactions and their impact on wave parameters. In: Proceedings of the European Wave and Tidal Energy Conference, 15. <https://doi.org/10.36688/ewtec-2023-279>.
- Tan, T., Venugopal, V., 2024. Characterisation of turbulence at sites with coexisting waves and currents: An analysis by empirical mode decomposition. *Ocean Eng.* 313, 119616. <https://doi.org/10.1016/j.oceaneng.2024.119616>.
- Tan, T., Venugopal, V., Sellar, B., 2023. Analysis of turbulence parameters for a tidal energy site in a wave-current environment ASME 2023 42nd International Conference on Ocean, Offshore and Arctic Engineering. <https://doi.org/10.1115/OMAE2023-104347>.
- The Treacherous and Productive Seas of Southern Africa 2017. <https://earthobservatory.nasa.gov/images/89535/the-treacherous-and-productive-seas-of-southern-africa> (accessed July 13, 2024).
- Tolman HL. User manual and system documentation of WAVEWATCH III TM version 3.14 n.d.
- TOMAWAC - Wave propagation in coastal areas n.d. <http://www.opentelemac.org/index.php/presentation?id=20> (accessed August 17, 2022).
- Vögler, A., Venugopal, V., 2013. Hebridean marine energy resources: wave-power characterisation using a buoy network. *Am. Society Mech. Eng. Digital Collection* 477–488. <https://doi.org/10.1115/OMAE2012-83658>.
- van der Westhuysen, A.J., Zijlema, M., Battjes, J.A., 2007. Nonlinear saturation-based whitecapping dissipation in SWAN for deep and shallow water. *Coast. Eng.* 54, 151–170. <https://doi.org/10.1016/j.coastaleng.2006.08.006>.
- van der Westhuysen, A.J., 2012. Spectral modeling of wave dissipation on negative current gradients. *Coast. Eng.* 68, 17–30. <https://doi.org/10.1016/j.coastaleng.2012.05.001>.
- Venugopal, V., Nemalidinne, R., 2014. Marine Energy Resource Assessment for Orkney and Pentland Waters With a Coupled Wave and Tidal Flow Model. Volume 9B: Ocean Renewable Energy. American Society of Mechanical Engineers, San Francisco, California, USA. <https://doi.org/10.1115/OMAE2014-24027>. V09BT09A010.
- Venugopal, V., Nemalidinne, R., 2015. Wave resource assessment for Scottish waters using a large scale North Atlantic spectral wave model. *Renew. Energy* 76, 503–525. <https://doi.org/10.1016/j.renene.2014.11.056>.
- Venugopal, V., Vögler, A., 2020. Modelling wave-current-turbulence interactions for tidal energy applications. In: Ocean Renewable Energy, Volume 9. American Society of Mechanical Engineers, Virtual, Online. <https://doi.org/10.1115/OMAE2020-19298>. V009T09A009.
- Venugopal, V., Nemalidinne, R., Vögler, A., 2017. Numerical modelling of wave energy resources and assessment of wave energy extraction by large scale wave farms. *Ocean Coast. Manage* 147, 37–48. <https://doi.org/10.1016/j.ocecoaman.2017.03.012>.
- Venugopal, V., Vögler, A., Sellar, B., 2018. Characterisation of Wave-Tidal Current-Turbulence Interactions at Tidal Energy Sites in the Orkney Islands.
- Webb, A., Waseda, T., Kiyomatsu, K., 2020. A high-resolution, long-term wave resource assessment of Japan with wave-current effects. *Renew. Energy* 161, 1341–1358. <https://doi.org/10.1016/j.renene.2020.05.030>.
- Wolf, J., Prandle, D., 1999. Some observations of wave-current interaction. *Coast. Eng.* 37, 471–485. [https://doi.org/10.1016/S0378-3839\(99\)00039-3](https://doi.org/10.1016/S0378-3839(99)00039-3).
- Yan, L., 1987. An Improved Wind Input Source Term For Third Generation Ocean Wave Modelling. *Wetenschappelijk Rapport = Scientific Report Koninklijk Nederlands Meteorologisch Instituut*.